Mononuclear Metal-O_2 Complexes

~ bearing macrocyclic TMC ligands ~

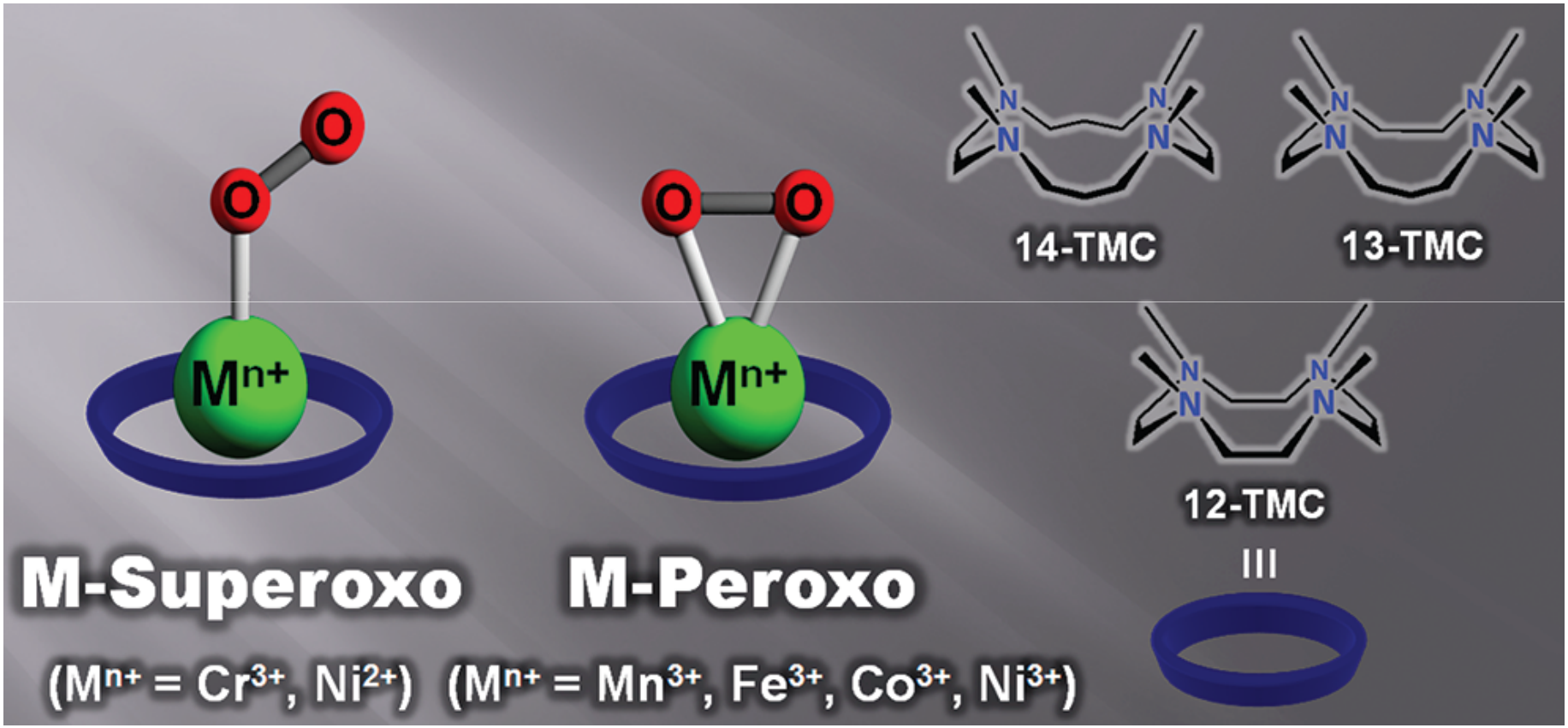

Nam, W et *al.* *Acc. Chem. Res. Early View.*

2012. 08. 27. Sonobe (D1)

Contents

Introduction

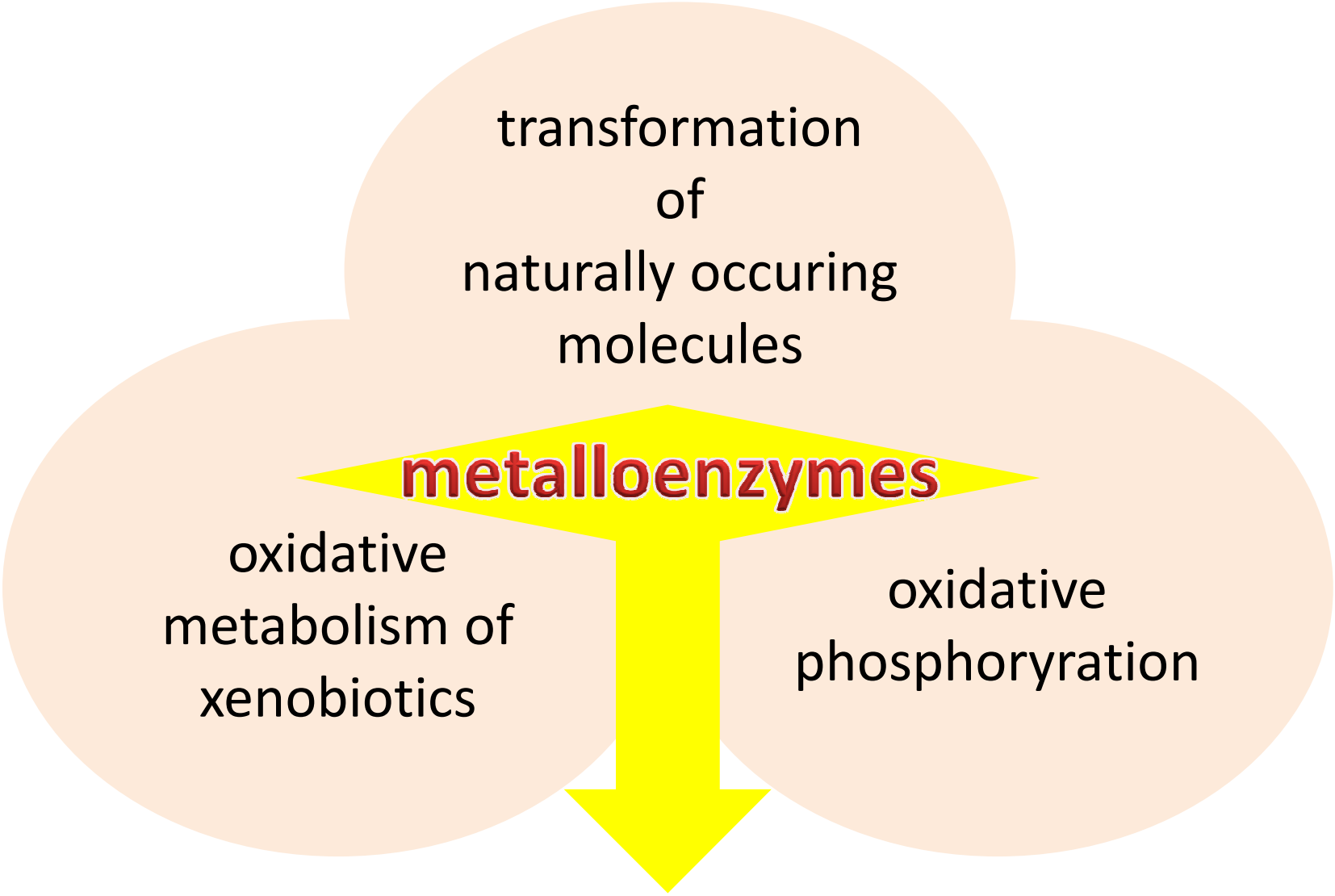

Introduction

metalloenzymes are well investigated
e.g. P450

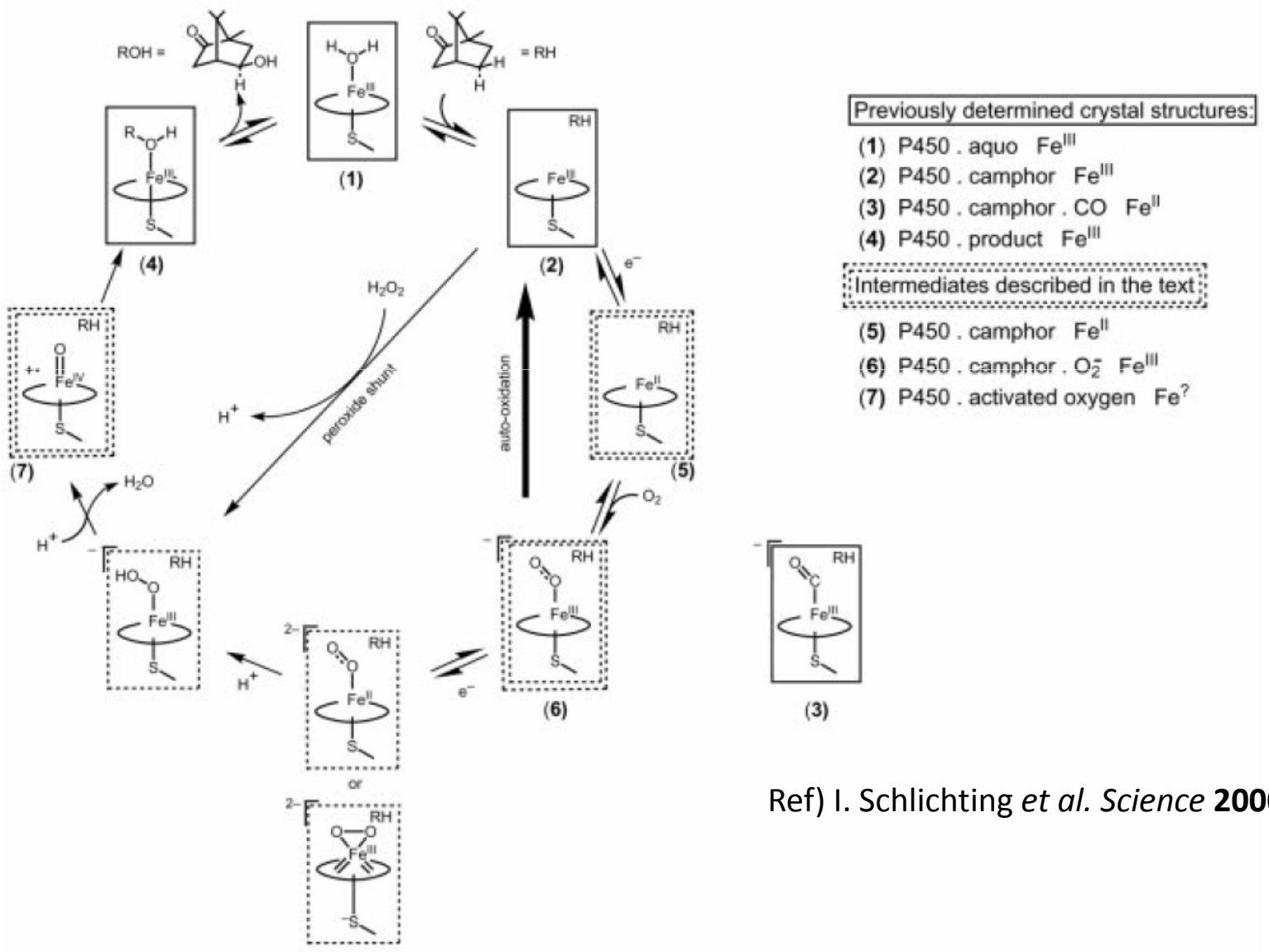

Ref) I. Schlichting *et al. Science* **2000**, *287*, 1615.

Introduction

Naphtalene dioxygenase

Ref) S. Ramaswamy *et al. Science* **2003**, *299*, 1039.

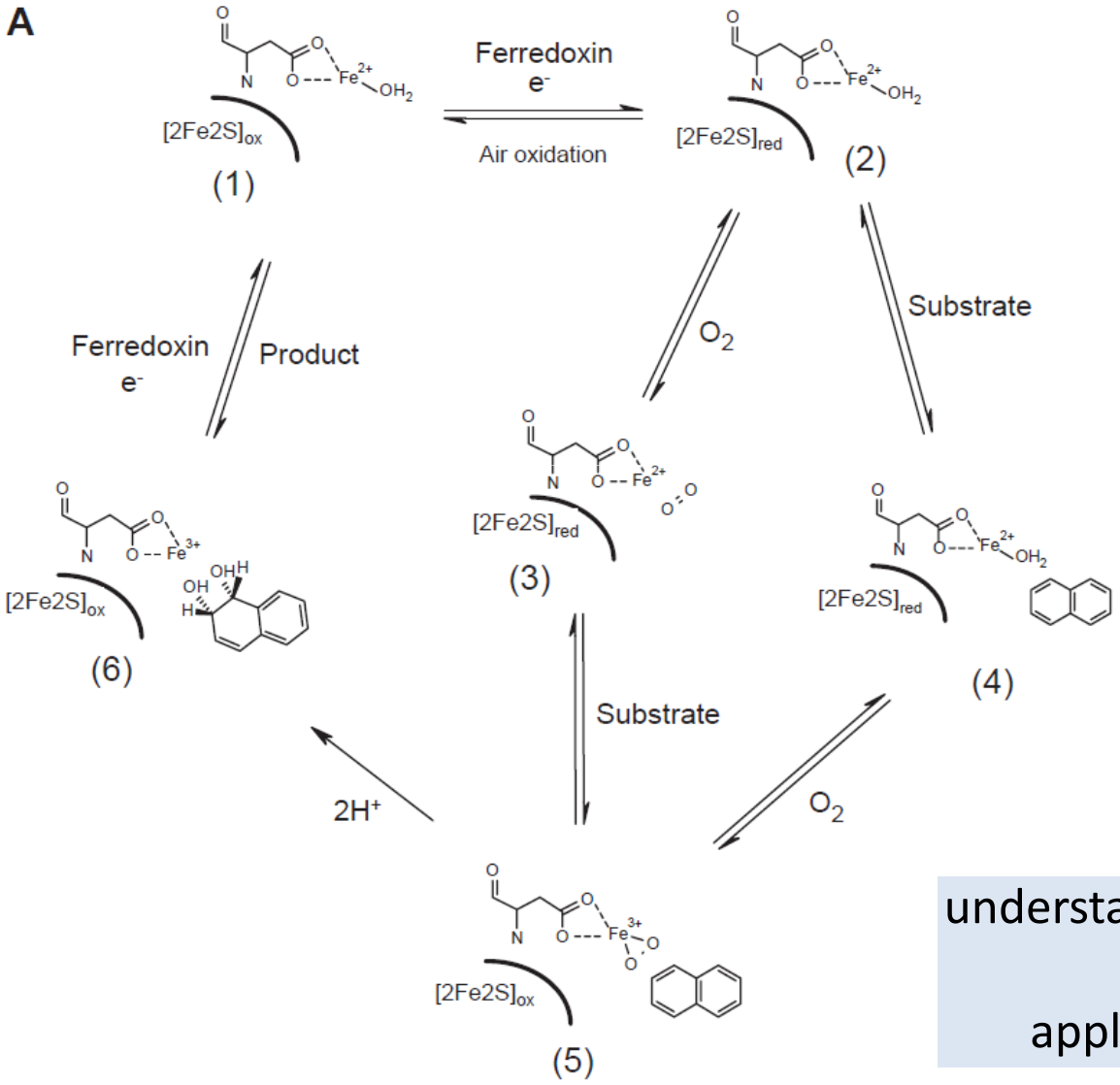

model study of M-O2

We can…

understand the O2 activation mechanisms

&

apply M-O2 to organic reaction !!

Contents

Synthesis of Metal-Superoxo and Peroxo Complexes

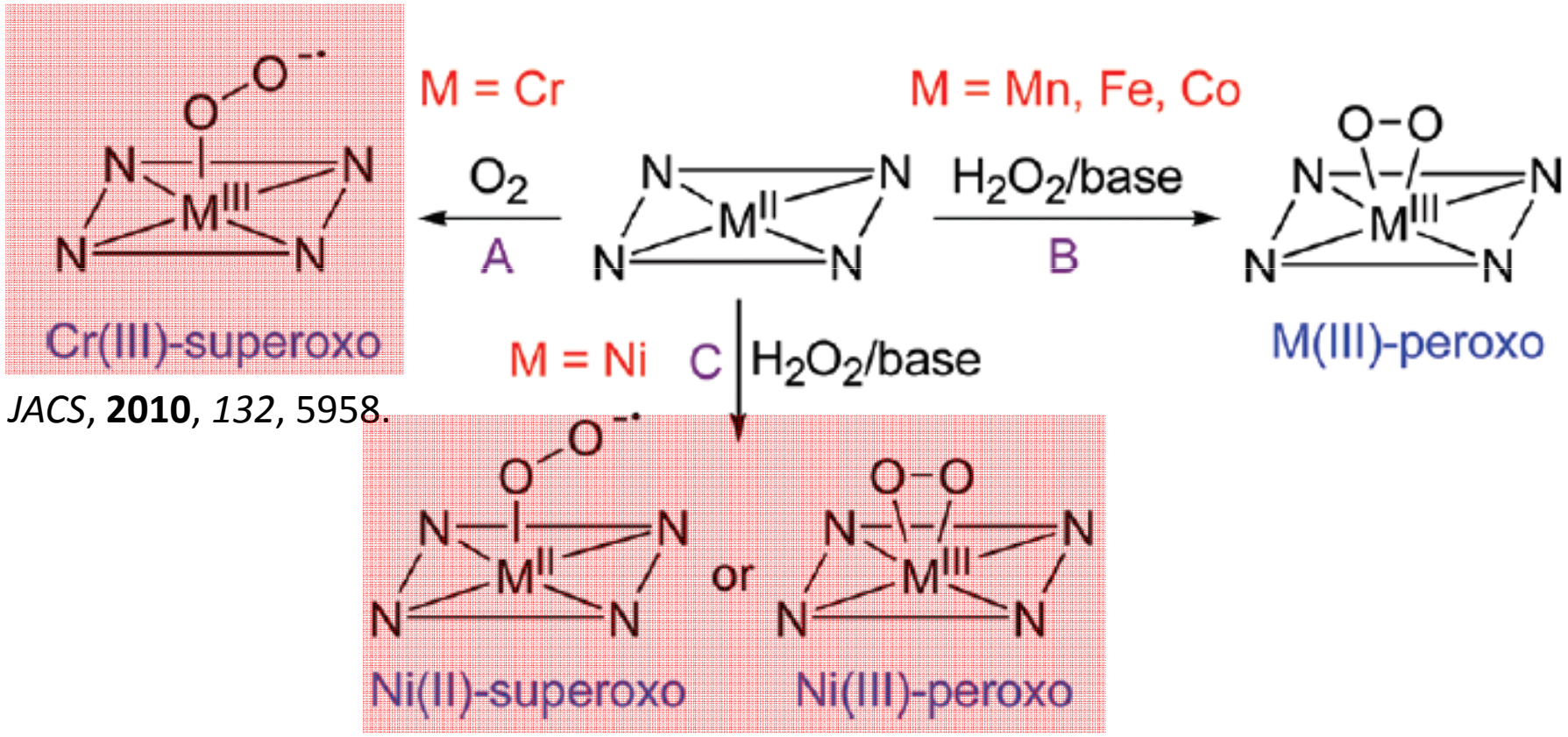

JACS, **2010**, *132*, 5958.

JACS, **2006**, *128*, 14230.

Nat. Chem. **2009**, *1*, 568.

Cr-O_2 complex

$CrCl_2$ (1.0 eq.) + 14-TMC (1.0 eq.) → (MeCN, Ar) $[Cr^{II}(14\text{-TMC})(Cl)]^+$ blue solid → (CH_3CN, O_2 bubbling, -10 °C) $[Cr^{III}(14\text{-TMC})(O_2)(Cl)]^+$ violet solid

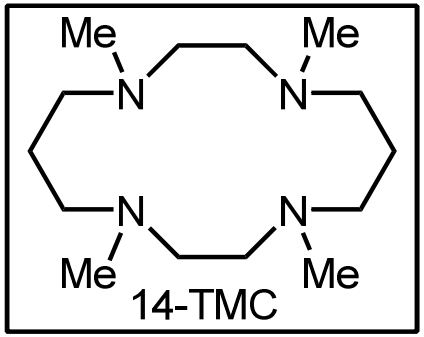

O-O bond length; 1.231(6) Å
(shorter than side-on Cr(III) complex; 1.327 Å)

Cr-O bond length; 1.876 Å
(shorter than side-on Cr(III) complex; 1.882 Å)

JACS. **2010**, *132*, 5958.

X-ray

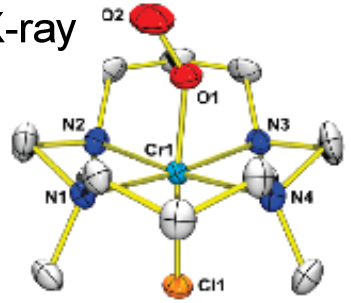

$[Cr^{III}(14^{-}TMC)(O_2)(Cl)]^+$

‘End-On’ Cr(III)-Superoxo Complex characterization

a) UV-vis absorptionspectra
&
resonance Raman spectra

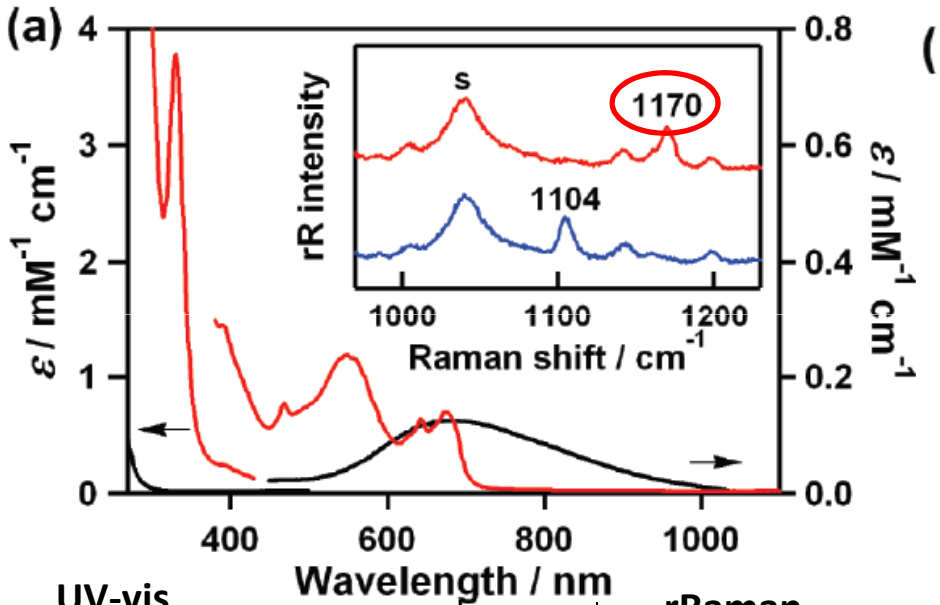

b) ESI-MS analysis

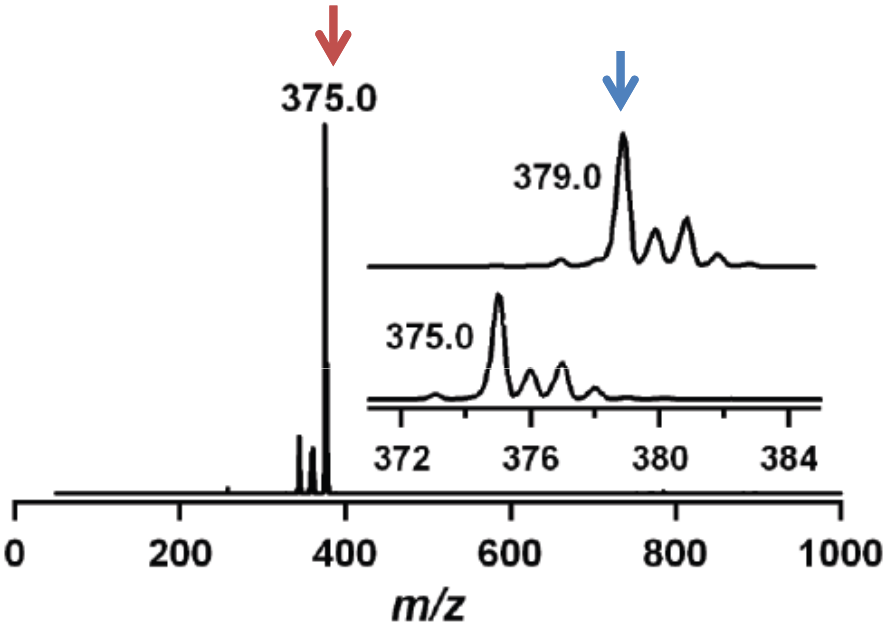

UV-vis

[Cr(14-TMC)(Cl)]$^{+}$

[Cr(14-TMC)(O2)(Cl)]$^{+}$

rRaman

$^{16}O_2$

$^{18}O_2$

[Cr(14-TMC)(^{16}O2)(Cl)]$^{+}$

[Cr(14-TMC)(^{18}O2)(Cl)]$^{+}$

O-O stretching vibration $^{16}\Delta$-$^{18}\Delta$ = 66 cm^{-1} (calculated $^{16}\Delta$-$^{18}\Delta$ = 67 cm^{-1})

[Cr^{III}(14-TMC)(O$_2$)(Cl)]$^{+}$: 1170 cm^{-1}

PNAS. **2003**, *100*, 3635.

reported Raman shift of end-on Cr(III)-superoxo complex [Cr(O$_2$)(H$_2$O)$_5$]$^{2+}$ = 1166 cm^{-1}

reported Raman shift of side-on Cr(III) complex [Tp^{tBu}Cr(pz'H)(O$_2$)]BARF = 1072 cm^{-1}

Ni-O2 complex

JACS. **2006**, *128*, 14230.

[Ni(14-TMC)](OTf)
blue

O_2 bubbling
or
H_2O_2 (10 eq.)
Et_3N (10 eq.)
O_2

O_2 bubbling

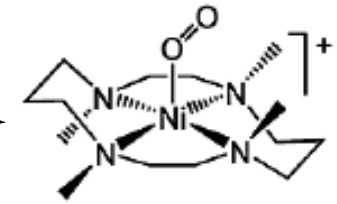

$[Ni(14^{-}TMC)(O_2)]^{+}$
green-brown

rRaman; 1131 cm-1
Ni^{2+}-superoxo
ESI-MS; 346.1 (calcd. 346.1)
350.0 $^{18}O_2$

XAS (X-ray absorption spectroscopy)
8333.9 eV -> characteristic of Ni^{2+}

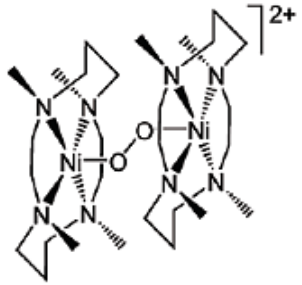

Ni-O-O-Ni
red

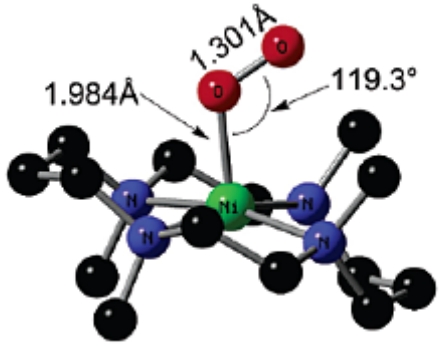

DFT optimized structure

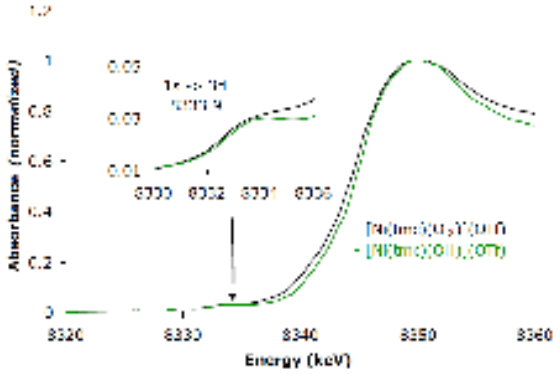

EXAFS; Ni-O 1.984 Å -> end-on

Nat. Chem. **2009**, *1*, 568.

$Ni(ClO_4)_2.6H_2O$ (1.2 eq.) + 12-TMC (1.0 eq.) → MeCN, reflux → $[Ni(12^{-}TMC)(CH_3CN)]^{2+}$ purple solid

H_2O_2 (5 eq.)
Et_3N (2 eq.)
MeCN, 0 °C

→ $[Ni(12^{-}TMC)(O_2)]^{2+}$ green solid

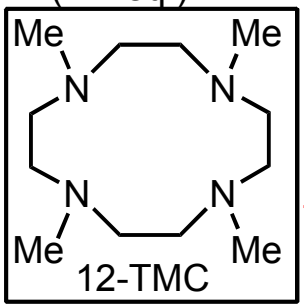

distorted octahedral geometry
(∠O-Ni-O= 43.04°)
O-O bond length; 1.386(4) Å
Ni-O bond length; 1.889 Å
this complex persist several days at 25 °C!!

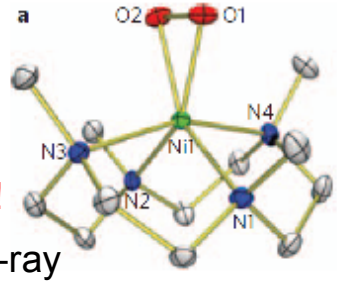

X-ray

0

side-on Ni(12-TMC)-O_2 complexes characterization

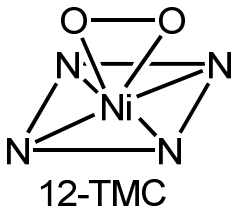

12-TMC

ESI-MS; 318.0 (calcd 318.2)
^{18}O 322.0 (calcd. 322.2)
contains O_2 unit

Raman spectrum (442 nm)

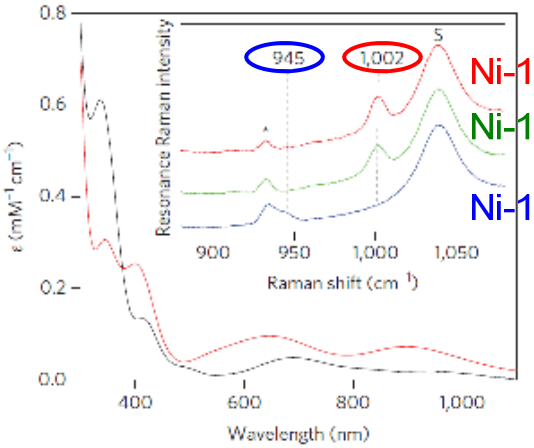

O-O frequency 1002 cm^{-1}
peroxo < Ni-O_2 < superoxo
800-900 1050-1200

XAS (X-ray absorption spectroscopy)

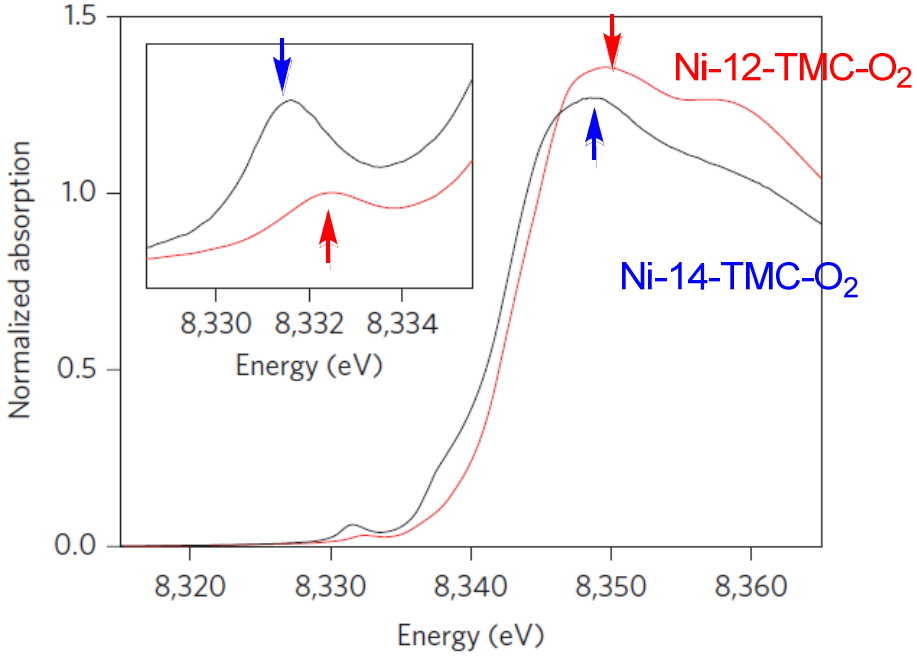

pre-edge
Ni-14-TMC-O_2; 8331.6 eV
Ni-12-TMC-O_2; 8332.3 eV
increased ligand field energy
-> Ni^{3+}

EXAFS
Ni-14-TMC-O_2; 8346.6 eV
Ni-12-TMC-O_2; 8344.8 eV
maximum shift ~ 1.8 eV
Ni-O; 1.978 Å -> side-on

DFT calulation of Ni(nTMC)-O_2 complexes

optimized structures with DFT calculation

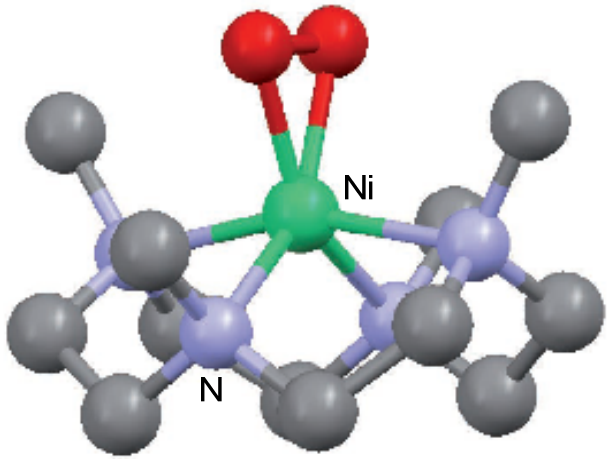

$[Ni(12^-TMC)(O_2)]^{2+}$

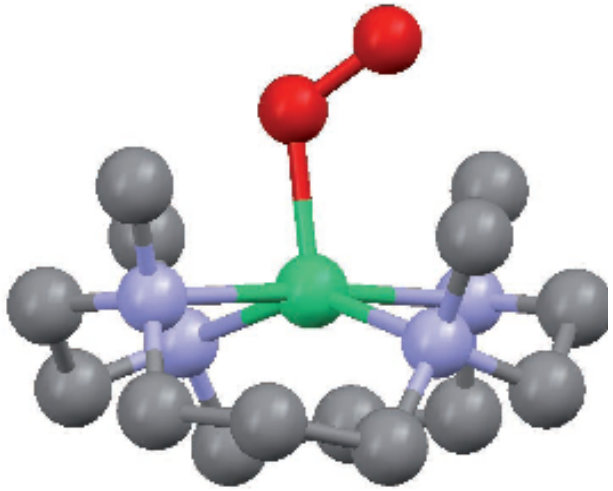

$[Ni(14\text{-}TMC)(O_2)]^{2+}$

small size ligand displace Ni out of N-plane

⇩

allowing facile side-on overlap with O_2

side-on mode can strongly overlap with Ni $3d_{x2-y2}$ orbital and O_2 π^*

	Structural Parameters						Mayer Bond Order		Mulliken Population $Ni(O_{Total})^b$		
	Ni O_1 (O_2)	O_1-O_2	Ni N_1 (N_2)[a]	NiO_1O_2	NiN_1N_2	NiN_2N_1	Ni-O_1	O_1-O_2	1	2	3
$[Ni(12^-TMC)(O_2)]^{2+}$	1.88 (1.88)	1.40	2.06 (2.19)	68.2	160.3	109.8	0.7	0.83	34.1 (55.5)	68.3 (2.1)	45.6 (43.2)
$[Ni(14\text{-}TMC)(O_2)]^{2+}$	1.96 (2.83)	1.30	2.14 (2.17)	120.3	149.2	174.8	1.22	0.86	5.6 (90.5)	47.5 (37.4)	71.9 (3.0)

Synthesis of Metal-Superoxo and Peroxo Complexes

Co complex: *Inorg. Chem*. **2008**, *102*, 2155.
JACS, **2010**, 132, 16977.

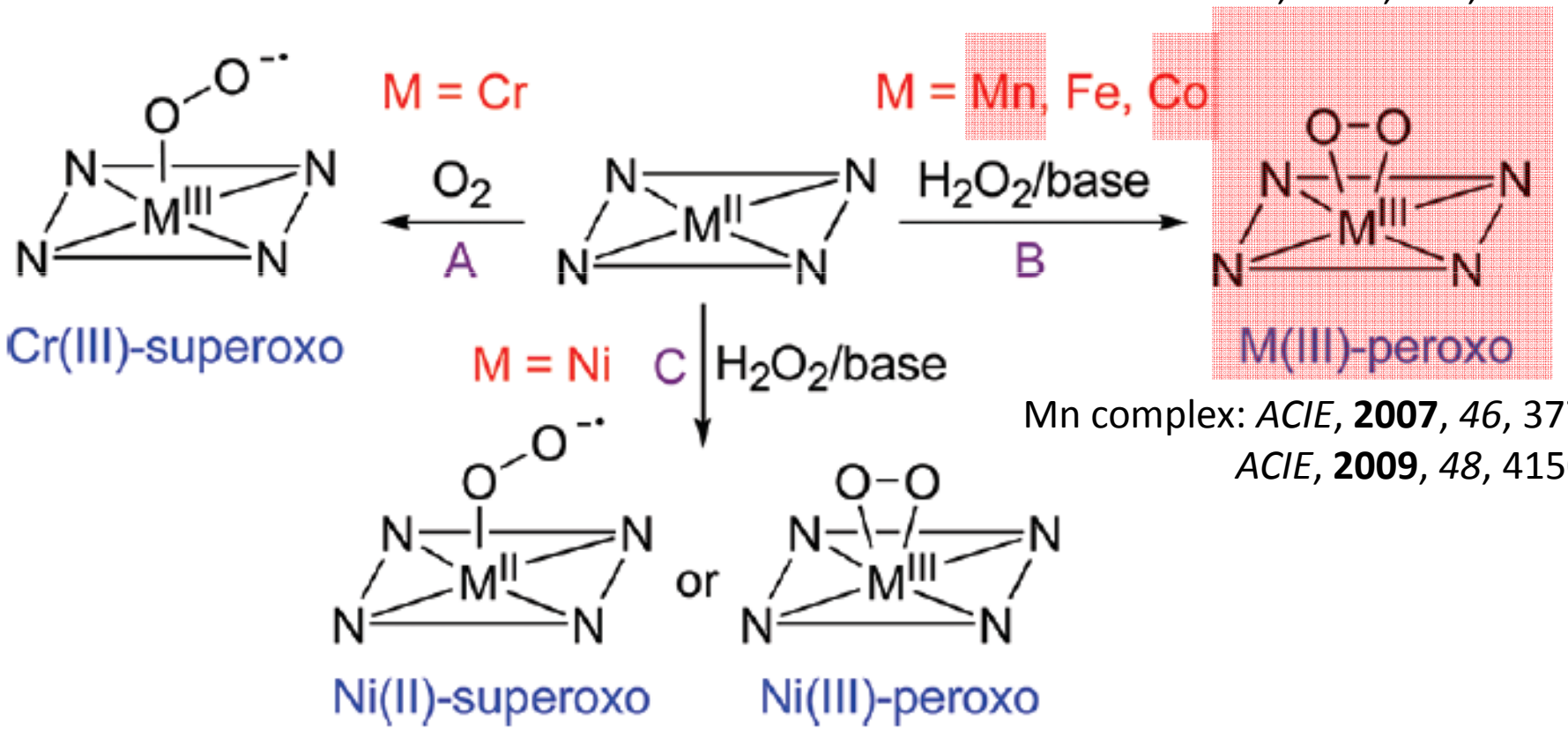

Mn complex: *ACIE*, **2007**, *46*, 377.
ACIE, **2009**, *48*, 4150.

‘Side-On’ Mn(III)-peroxo Complex synthesis & characterization (Mn(14-TMC)(O_2)-complex

$MnCl_2$ + $TMS(CF_3SO_3)_2{\cdot}2CH_3CN$ —(CH_3CN, in Glove Box)→ $Mn(CF_3SO_3)_2{\cdot}2CH_3CN$ (1.2 eq.) —(14-TMC (1.0 eq.), CH_3CN)→ $Mn(14\text{-}TMC)(CF_3SO_3)_2{\cdot}2CH_3CN$ 70% yield.

$Mn(14\text{-}TMC)(CF_3SO_3)_2{\cdot}2CH_3CN$ —(H_2O_2 (5.0 eq.), Et_3N (2.5 eq.), CH_3CN, rt, 30 sec)→ $[Mn(14\text{-}TMC)(O_2)]^+$

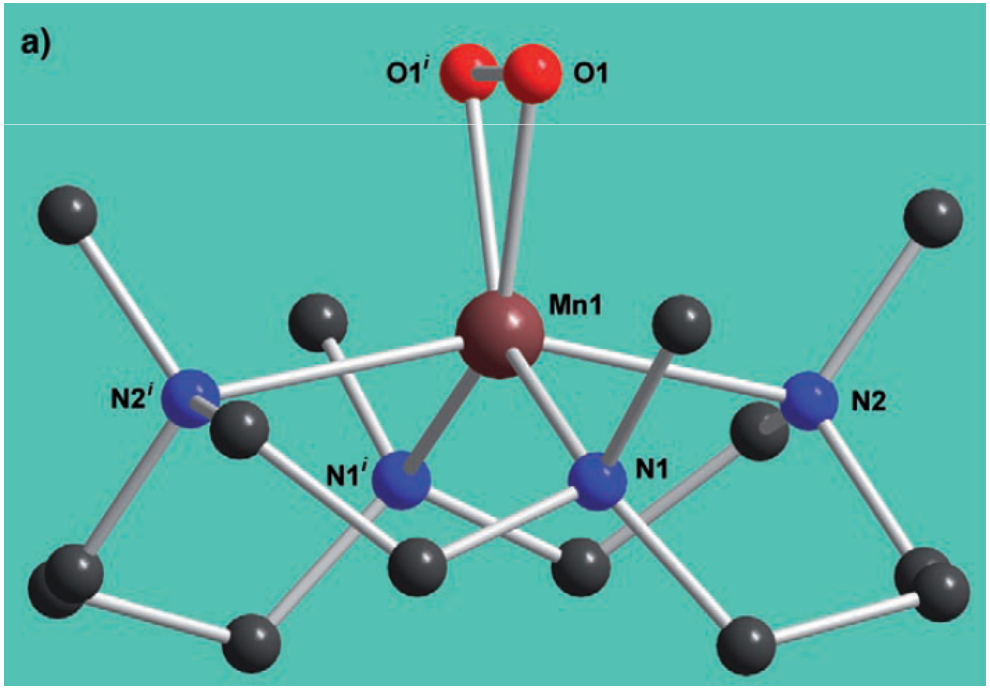

$[Mn(14\text{-}TMC)(O_2)]^+$

bond length

O-O; 1.403(4) Å
(slightly shorter than $[Mn(tpp)(\eta^2\text{-}O_2)]^-$; 1.43 Å)
Mn-O; 1.884(2) Å, Mn-N; 2.265(4) Å
-> good agreement with other Mn^{III} complexes

geometry

Mn ion is very distorted octahedral.
N-Me groups are oriented syn to the peroxo ligand.

ESI-MS

343.1 (calcd 343.2)
$^{18}O_2$; 347.1 (calcd 347.2)
contain O_2 unit

This complex persisted several hour @ 25 ^oC !

‘Side-On’ Mn(III)-peroxido Complex synthesis & characterization (Mn(14-TMC)(O_2)-complex

EPR analysis

$[Mn(tmc)]^{2+}$

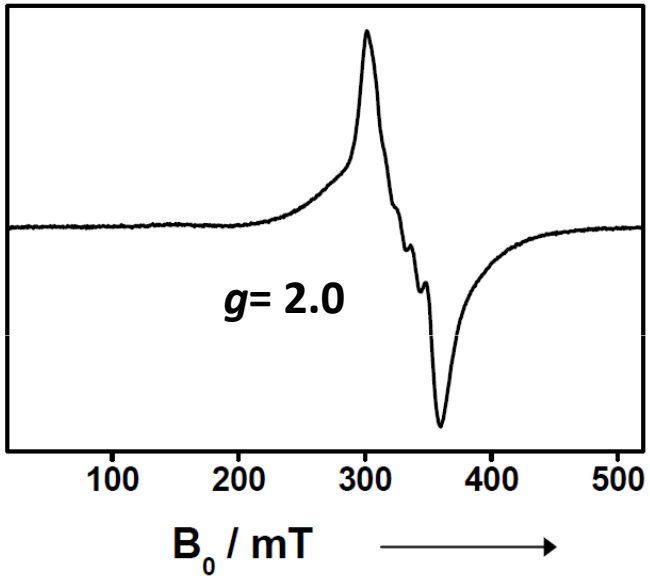

(S= 5/2) Mn(II) species

$[Mn(tmc)(O_2)]^{+}$

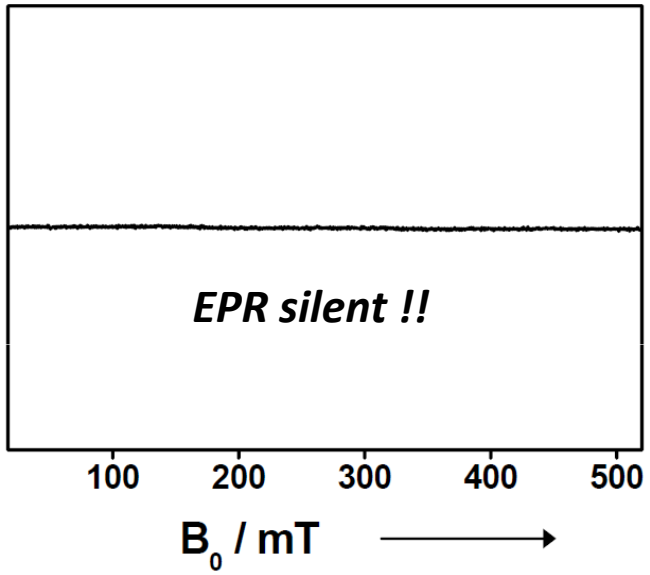

d^4 species; high-spin (S=2) or low-spin (S=1) ??

---

determination of spin state by HNMR spectroscopic method

(Evans method; *J. Chem. Soc.* **1959**, 2003.; *J. Chem. Soc. Dalton Trans*. **1998**, 2927.)

$$\mu = 0.0618(\Delta\nu T/2f \cdot M)^{1/2}$$

f **; the oscillator frequency (MHz)**
T **; absolute temperature**

M **; molar concentration of the metal ion**
$\Delta\nu$ **; the difference of frequnecy (Hz) between the two reference signals**

5.4μ_B

high spin state

‘Side-On’ Mn(III)-peroxido Complex synthesis & characterization (Mn(13-TMC)(O_2)-complex)

$$[Mn(13\text{-}TMC)](CF_3SO_3)_2 \xrightarrow[CH_3CN,\ 10\ ^oC]{H_2O_2\ (5.0\ eq.),\ Et_3N\ (2.5\ eq.)} [Mn^{III}(13\text{-}TMC)(O_2)]^+$$

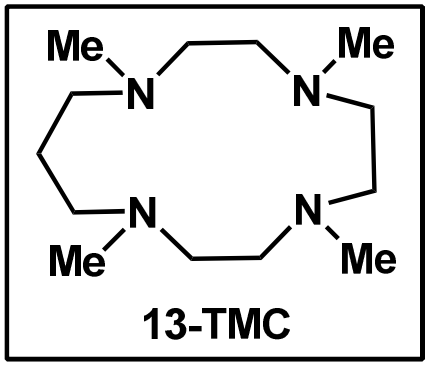

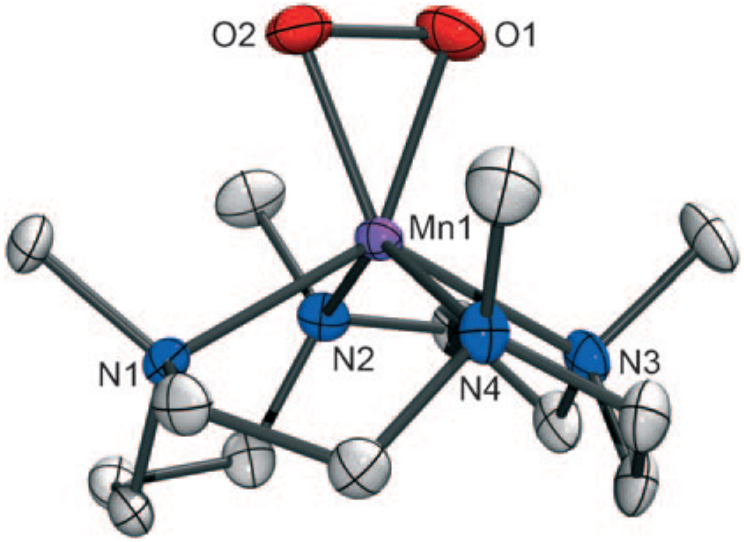

bond length

O-O ; 1.410(4) Å (typical but slightly longer than Mn(14-TMC)(O_2))
Mn-O ; 1.859 Å (shorter than Mn(14-TMC)(O_2))

geometry

nominally octahedral geometry of Mn ion center
very distorted

Mn-O_2 bite angle

small bite angle ; (44.55(11)^o)

‘Side-On’ Co(III)-peroxo Complex synthesis & characterization

$Co(OTf)_2{\cdot}6H_2O$ + 14-TMC $\xrightarrow[CH_3CN,\ Ar]{}$ $Co^{II}(TMC)(CH_3CN)^{2+}$ $\xrightarrow[CH_3CN,\ 0\ ^oC]{H_2O_2\ (5\ eq.)\ \ Et_3N\ (2.5\ eq.)}$ $[Co^{III}(TMC)(O_2)]^+$

Inorg. Chem. **2008**, *102*, 2155.

peroxo complex

UV-vis ----comparable to the reported side-on $Co^{III}N_4O_2$

λ_{max} = 436 nm
575 nm
801 nm

Inorg. Chem. **2004**, *43*, 7558.

ESI-MS
$[Co(14\text{-}TMC)(^{16}O_2)]^+$; m/z= 347.1
$[Co(14\text{-}TMC)(^{18}O_2)]^+$; m/z= 351.1

EPR & NMR

$Co(TMC)(CH_3CN)^{2+}$; *g*= 7.13, 2.15, 1.51 ⟶ typical high spin (S=3/2) $Co^{II}(d^7)$

$[Co^{III}(TMC)(O_2)]^+$; EPR silent !! high spin (S=2) or (S=0) $Co^{III}(d_6)$

$Co(ClO_4)_2{\cdot}6H_2O$ + 12/13-TMC $\xrightarrow[CH_3CN,\ Ar]{}$ $Co^{II}(TMC)(CH_3CN)^{2+}$ $\xrightarrow[CH_3CN,\ 0\ ^oC]{H_2O_2\ (5\ eq.)\ \ Et_3N\ (2.5\ eq.)}$ $[Co^{III}(TMC)(O_2)]^+$

JACS, **2010**, *132*, 16977.

peroxo complex

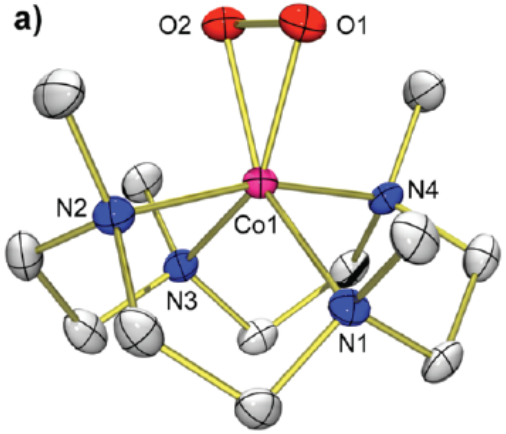

12-TMC

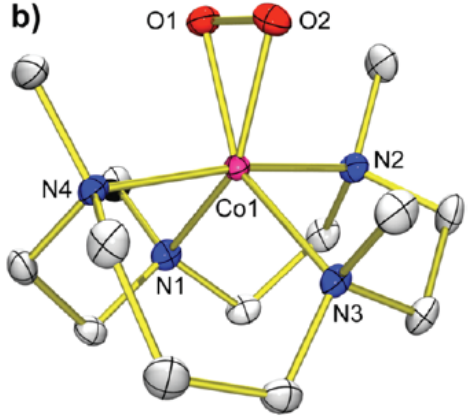

13-TMC

O-O length; 1.438(9) Å (12-TMC)
1.438(4) Å (13-TMC)
Co-O length; 1.866 Å
1.856 Å

(14-TMC-Ni-peoxo;1.386 Å
12/13-TMC-Co; 1.866 Å
12-TMC-Co; 1.889 Å)

CoO_2 angle ; 45.36°
45.16°

‘Side-On’ Co(III)-peroxo Complex synthesis & characterization

XAS analysis

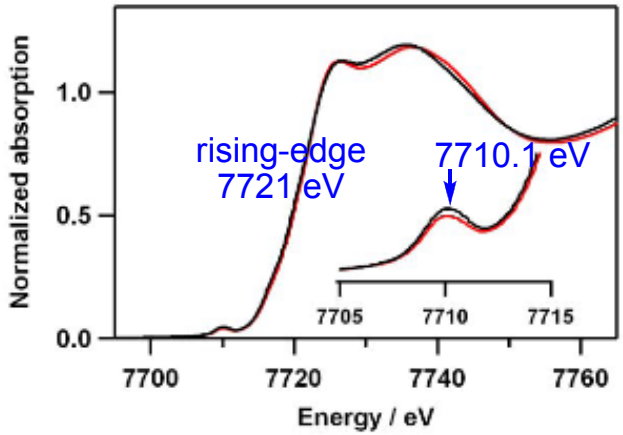

> pre-edge (7710.1 eV)
reflects ligand-field strength
> rising-edge (7721 eV)
reflects the charge at the absorbing metal center -> typical energy for Co^{3+}
> EXAFS
paremeter of both of the complexes are in good agreement with the crystal structure.

UV-vis

$[Co(12\text{-}TMC)(O_2)]^+$
λ_{max} = 350 nm
560 nm
shoulders at ~ 500, ~ 700 nm

$[Co(13\text{-}TMC)(O_2)]^+$
λ_{max} = 348 nm
562 nm
shoulders at ~ 500, ~ 710 nm

ESI-MS

$[Co(12\text{-}TMC)(^{16}O_2)]^+$; 319.1 (calcd 319.2)
$[Co(12\text{-}TMC)(^{18}O_2)]^+$; 323.1 (calcd 323.2)
$[Co(13\text{-}TMC)(^{16}O_2)]^+$; 333.1 (calcd 333.2)
$[Co(13\text{-}TMC)(^{18}O_2)]^+$; 337.1 (calcd 337.3)

Co(III)-O2 complexes exist as superoxo complexes in solid & solution state.

rRaman (442 nm)

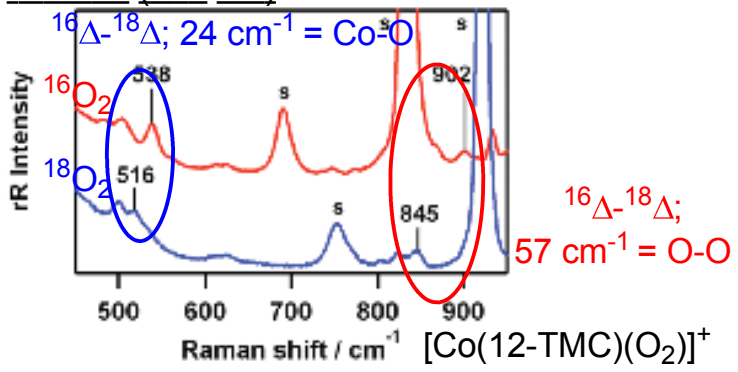

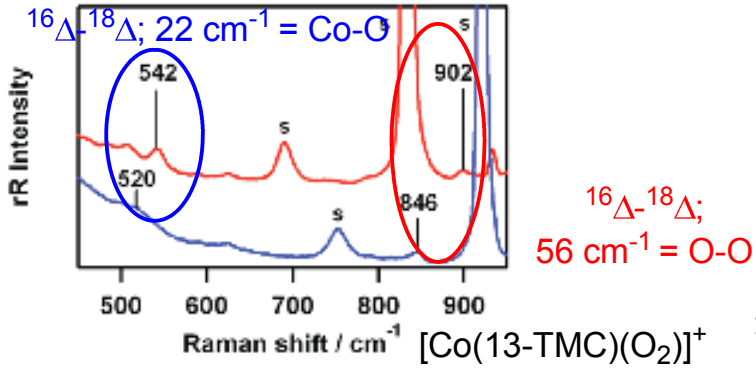

Co-(14-TMC)(O_2) is really side-on??

XAS

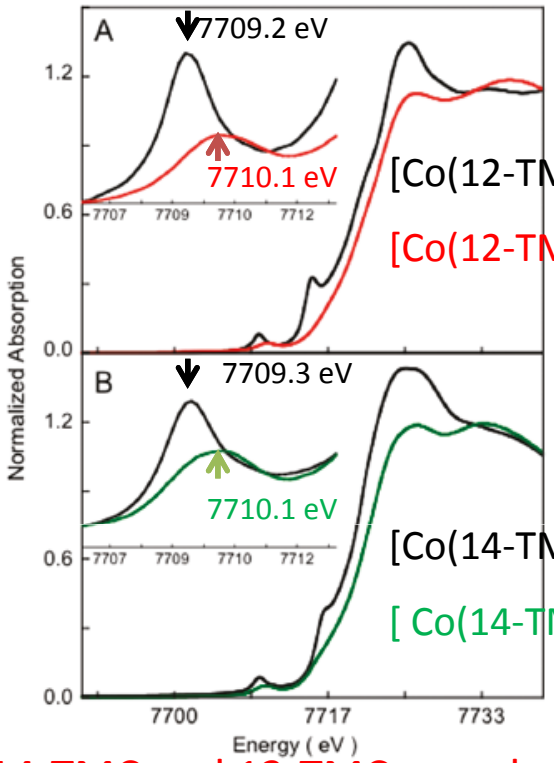

[Co(12-TMC)(O_2)]$^{+}$

[Co(12-TMC)(CH_3CN)]$^{2+}$

[Co(14-TMC)(O_2)]$^{+}$

[Co(14-TMC)(CH3CN)]$^{2+}$

14-TMC and 12-TMC complexes show Co^{3+}

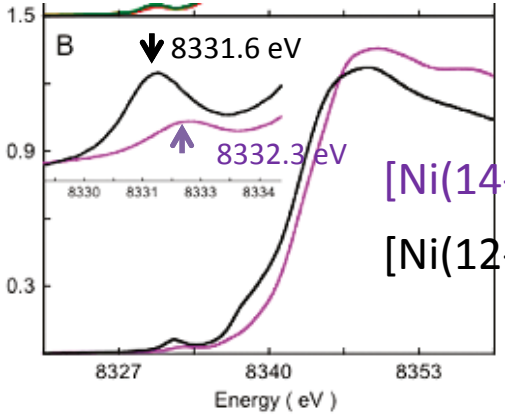

[Ni(14-TMC)(O2)]$^{+}$

[Ni(12-TMC)(O2)]$^{+}$

Ni^{2+}

Ni^{3+}

DFT calculation

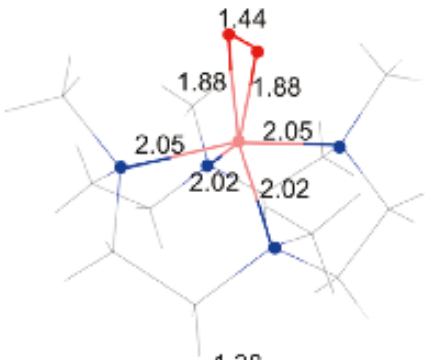

[Co(12-TMC)(O_2)]

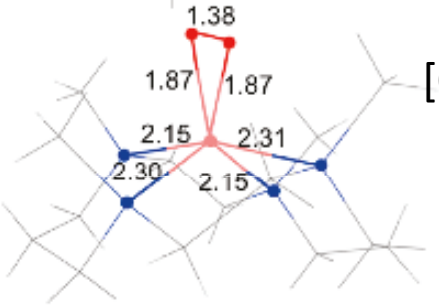

[Co(14-TMC)(O_2)]

14-TMC and 12-TMC complexes are side-on

11.5 kcal/mol higher

DFT calculation

[Ni^{II}(14-TMC)(O_2^-)]

[Co^{II}(14-TMC)(O_2^-)]

calc.

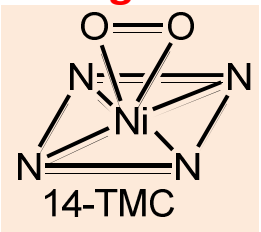

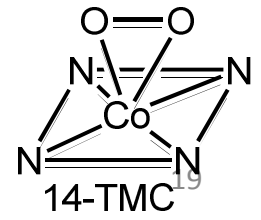

Synthesis of Metal-Superoxo and Peroxo Complexes

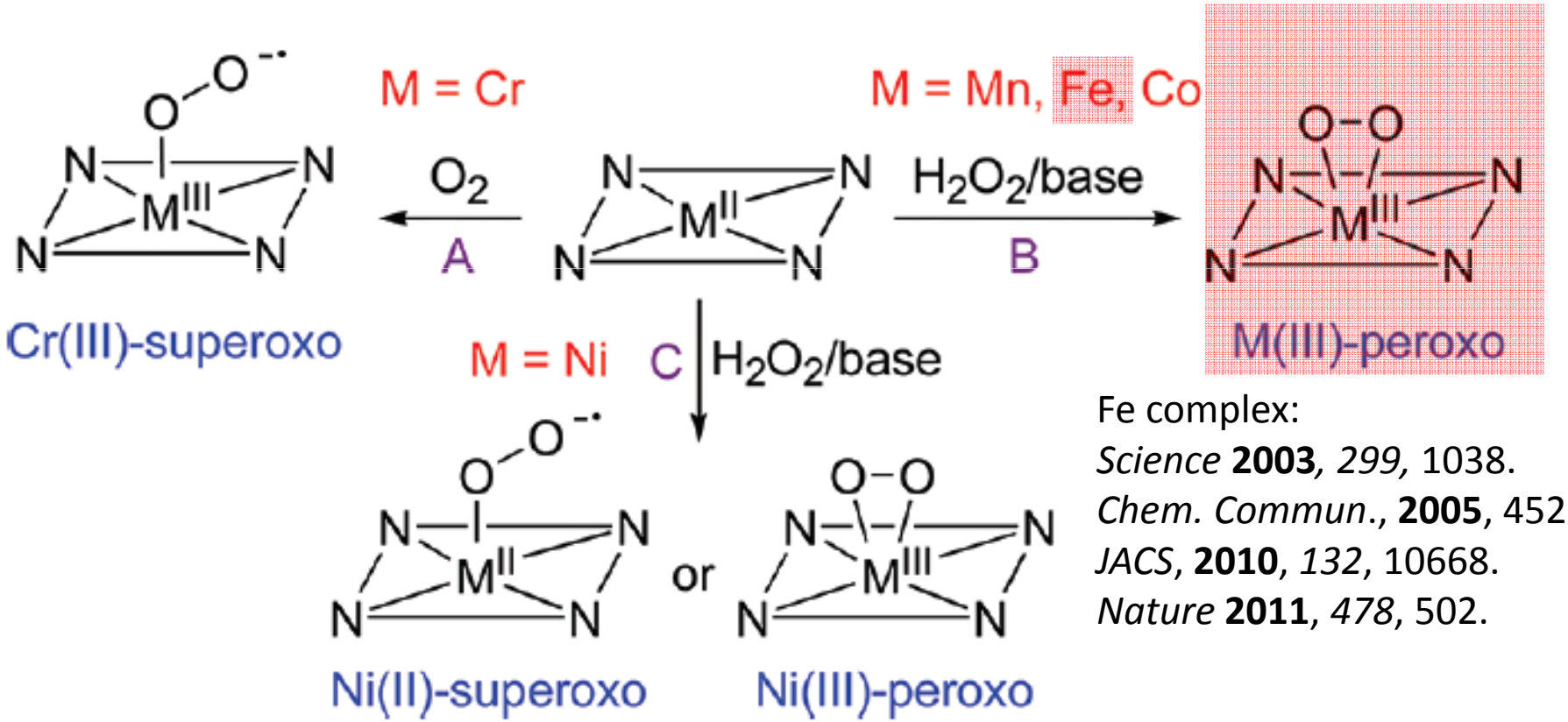

Fe complex:

Science **2003**, *299,* 1038.

Chem. Commun., **2005**, 4529.

JACS, **2010**, *132*, 10668.

Nature **2011**, *478*, 502.

Fe=O Complex
syntheis & charactrization

$Fe(OTf)_2{\cdot}2CH_3CN$ (1.0 eq.) + 14-TMC (1.0 eq.) → (CH_3CN, 12 h, inert gas) → $[Fe^{II}(TMC)(OTf)_2]$ (70 %) → (PhI=O (1.0 eq.) or H_2O_2 (3.0 eq.), CH_3CN, -40 °C) → $[Fe^{IV}(O)(TMC)(NCCH_3)](OTf)_2$ (90 %)

stable for 1 month @ -40 °C

Science **2003**, *299*, 1038.

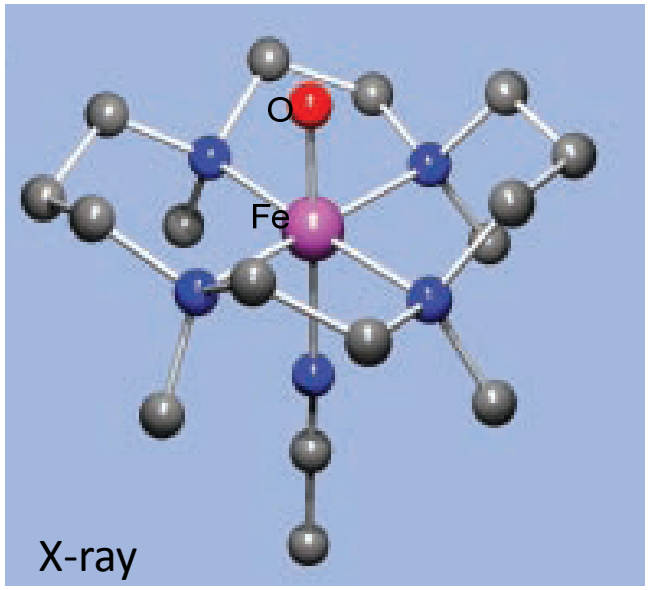

UV-vis ; λ_{max}= 820 nm

ESI-MS ; obs 476.9
$[Fe(IV)(O)(14\text{-}TMC)(OTf)]^+$

rRaman ;
$^{16}O_2$: 834 cm-1
$^{18}O_2$: 800 cm-1

bond length

Fe=O ; 1.646(3) Å - - closely match much shorter than Fe^{III}-O (1.813 Å $[Fe^{III}O(L)]^{2-}$; *Science* 2000, *289*, 938)

geometry

TMC coordinates to Fe in the plane perpendicular to the Fe=O axis, with the Fe slightly out of the plane defined by N_1~$_4$ toward the acetonitrile ligand by 0.0324 Å.

All N-Me pont away from oxo ligand.

Fe, O, $NCCH_3$ are nearly collinear.

porphyrin complexes

- - $r_{Fe\text{-}O}$:1.62-1.67 Å (*JACS*, 1986, *108*, 7819.)

cytochrome c peroxidase

2.2-2.5 Å (*Structure* 1994, *2*, 210.)

cytchrome P450

1.65-1.9 Å (*Science* 2000, *287*, 1615.)

(determinned by XAS)

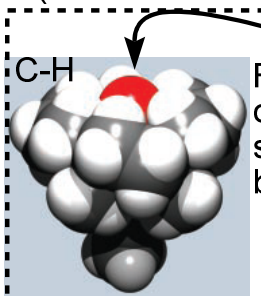

Fe=O is nestled in a bed of six C-H and self-distraction is inhibited by these C-H groups.

reason of stability

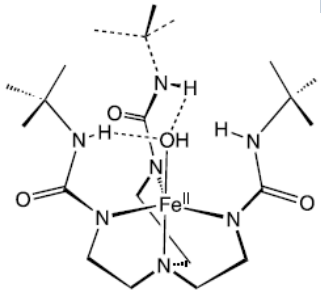

$[Fe(II)H_3\mathbf{1}(OH)]^{2-}$

$[Fe(III)O(L)]^{2+}$

Fe=O & Fe-O_2 Complexes syntheis & charactrization

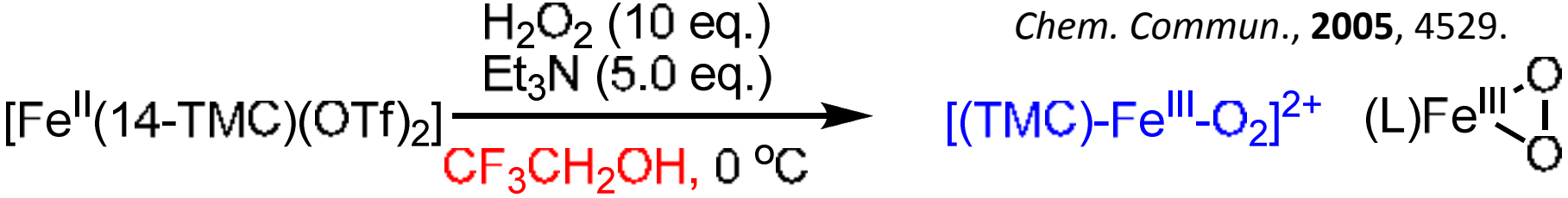

Chem. Commun., **2005**, 4529.

UV-vis

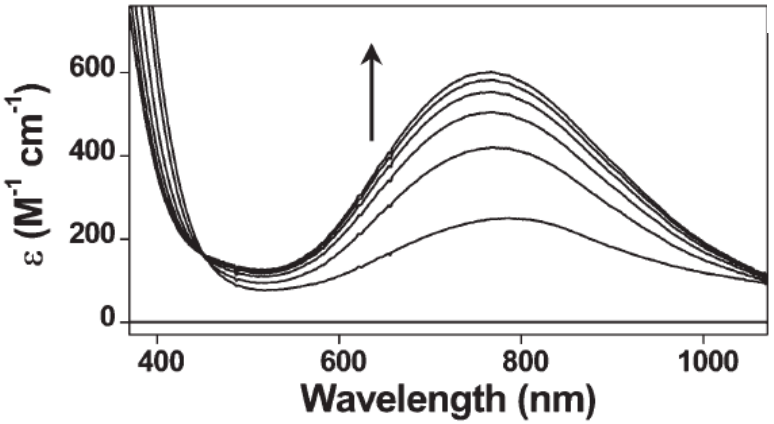

ESI-MS

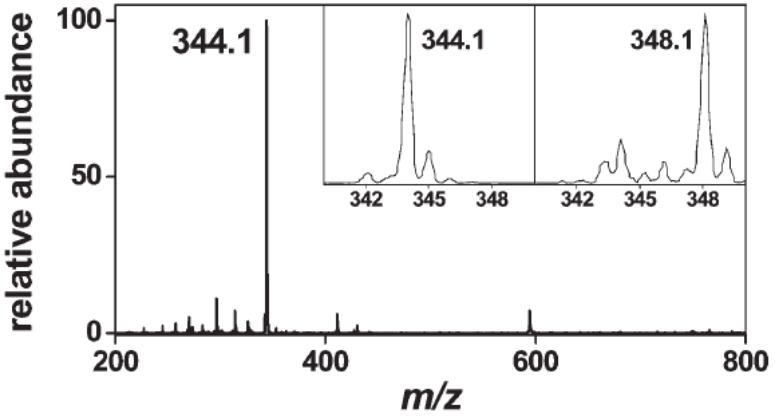

EPR

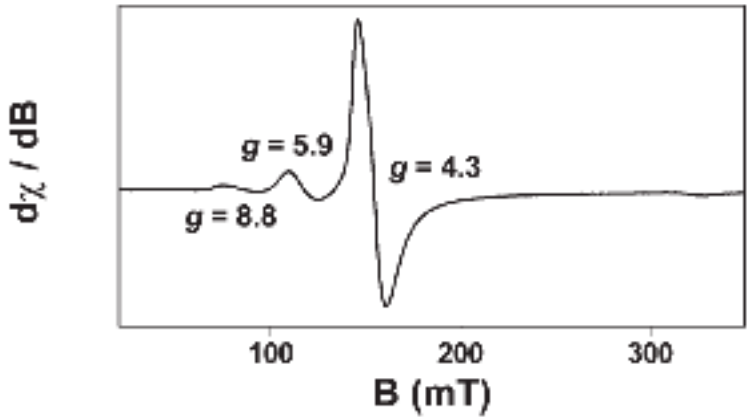

UV-vis; 750 nm

ESI-MS; found 344.1

calculated 344.1

^{18}O-labeled complex; 348.1

X-band EPR; typical of a high-spin (S=5/2) Fe(III) species

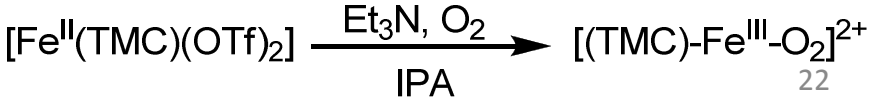

Fe=O & Fe-O_2 Complexes syntheis & charactrization (**dioxygen activation**)

JACS, **2005**, *127*, 4178.
JACS, **2009**, *131*, 13910.

$Fe^{II}(14\text{-TMC})(OTf)_2 \xrightarrow[CH_3CN]{O_2}$ no spectral change

$Fe^{II}(14\text{-TMC})(OTf)_2 \xrightarrow[CH_3CN \text{ w/ cosolvent}\ v/v=1/1]{\text{air}}$ pale green intermediate

λ_{max}; 825 nm (ε= 370 $M^{-1}cm^{-1}$)

⇩

$[(TMC)\text{-}Fe^{IV}{=}O]^{2+}$

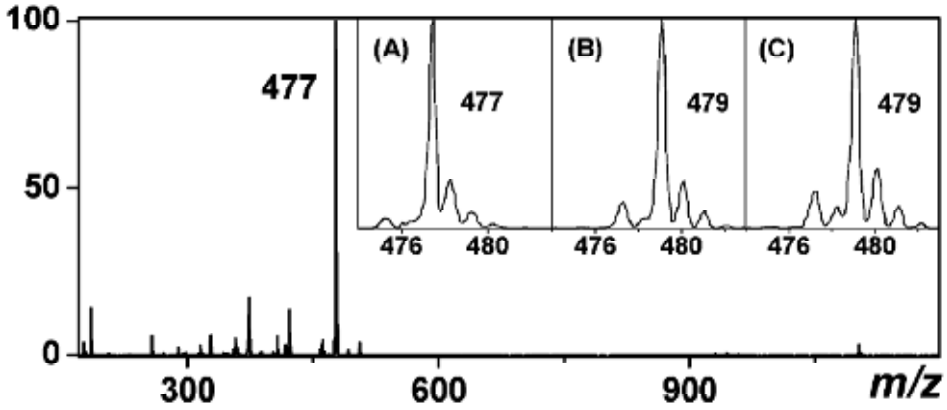

(A) mixed Fe-TMC complex and $^{16}O_2$
m/z; 477 $[Fe^{IV}(^{16}O)(TMC)(OTf)]^+$

(B) mixed Fe-TMC complex and $^{18}O_2$
m/z; 479 $[Fe^{IV}(^{18}O)(TMC)(OTf)]^+$

(C) mixed Fe-TMC complex and $^{16}O_2$ followed by addition of $H_2{}^{18}O$

$[(TMC)\text{-}Fe^{IV}{=}O]^{2+}$ exchanges its oxygen with H_2O at a first rate.

Fe=O & Fe-O_2 Complexes syntheis & charactrization

JACS, **2010**, *132*, 10668.

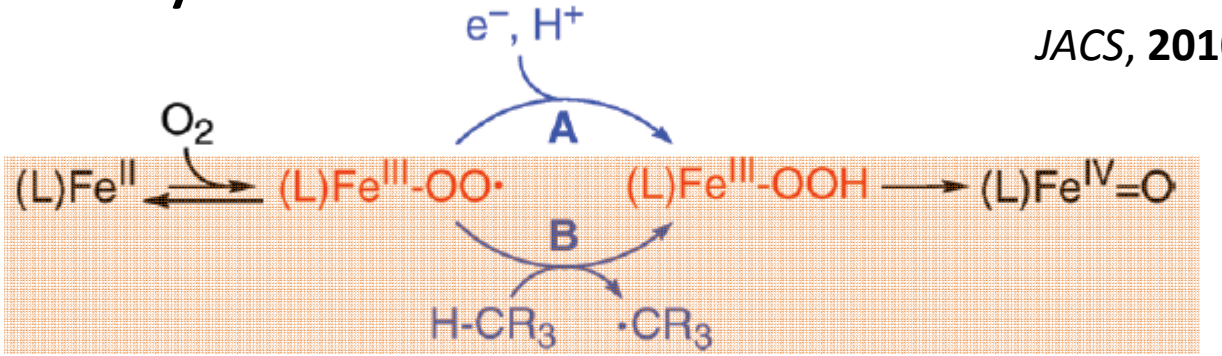

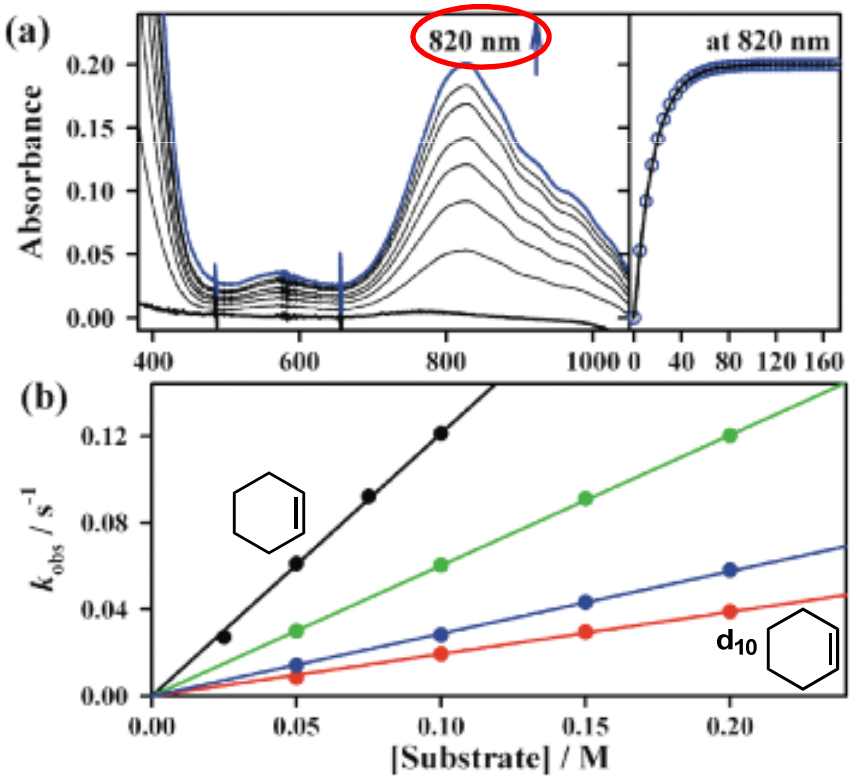

KIE value; 6.3

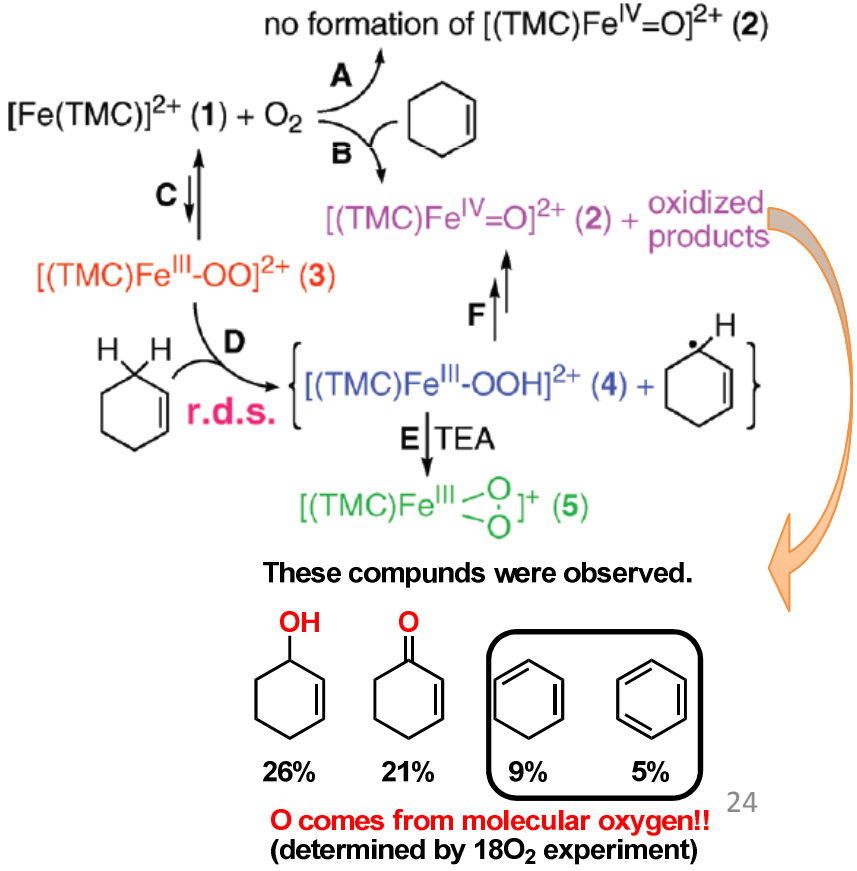

Fe=O & Fe-O_2 Complexes syntheis & charactrization

Nature **2011**, *478*, 502.

$$Fe(TMC)(OTf)_2 + H_2O_2\ (5.0\ eq.) \xrightarrow[CF_3CH_2OH,\ 0\ ^oC]{Et_3N\ (2.0\ eq.)} [Fe(TMC)(O_2)]^+$$

first report of Fe(III) peroxo structure

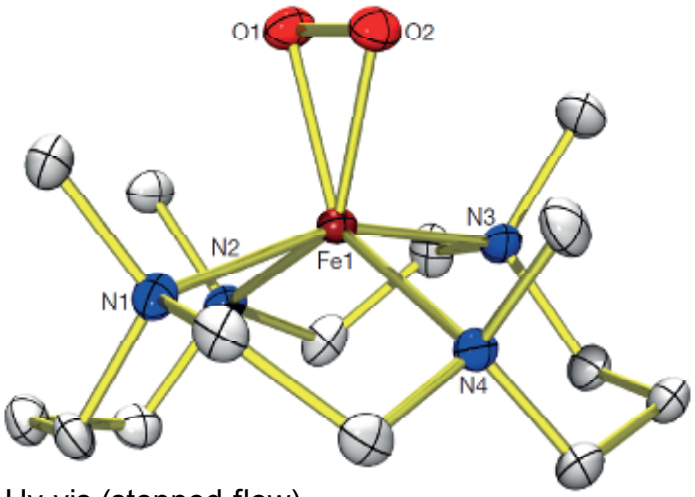

bond length

O-O ; 1.463(6) Å
Fe-O ; 1.910 Å
longer than those of (TMC)-Fe-peroxo complexes.

geometry

all n-Me groups point to the same side of the peroxo moiety, as observed in other M^{III}-peroxo complexes.
No axial ligand binds to Fe trans to the peroxo ligand.

UV-vis

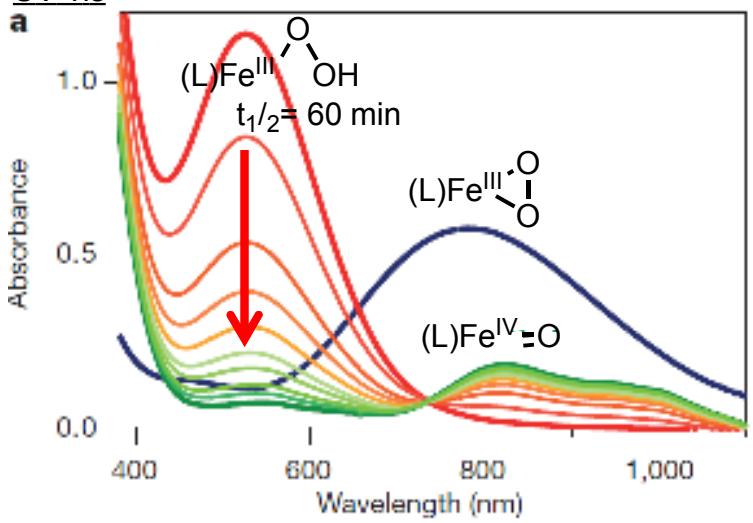

Uv-vis (stopped-flow)

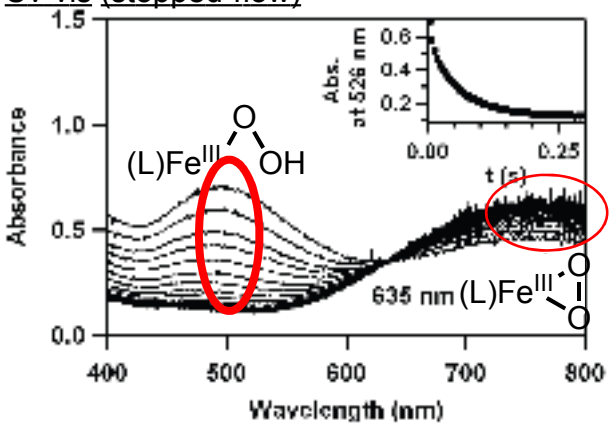

782 nm immediately dissapeared but 526 nm gradualy appeared.

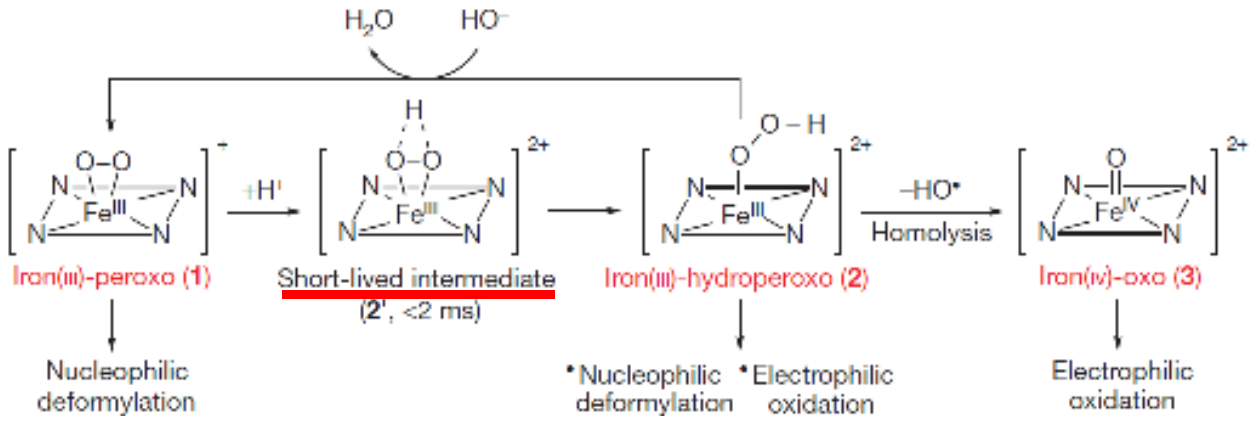

Fe=O & Fe-O_2 Complexes charactrization of Fe-OOH

EPR

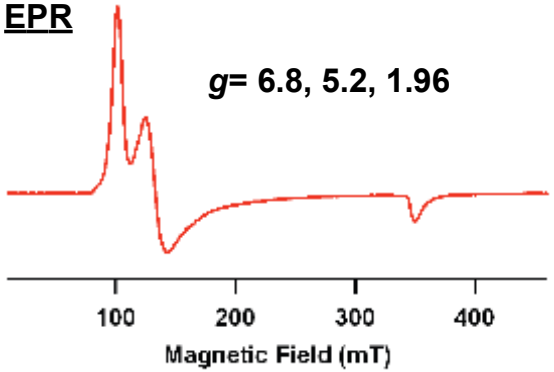

first shell EXAFS

Complex	Fit #	Path	CN	R(Å)	σ^2 (Å^2)	ΔE_0	Error
2	2-1	Fe-O	2	1.89	2495	-3.7	0.81
		Fe-N	4	2.17	527		
	2-2	Fe-O	1	1.85	526	-1.5	0.72
		Fe-N	4	2.17	584		

Fe K pre-edge energy and intensity fit values

	Peak 1 (eV)	Area	Peak 2 (eV)	Area	Total Intensity
[Fe(III)(TMC)(OO)]$^+$ (**1**)	7112.7	11.9	7114.4	5.6	17.5 ± 1.9
[Fe(III)(TMC)(OOH)]$^{2+}$ (**2**)	7112.9	19.0	7114.3	6.6	25.6 ± 2.3

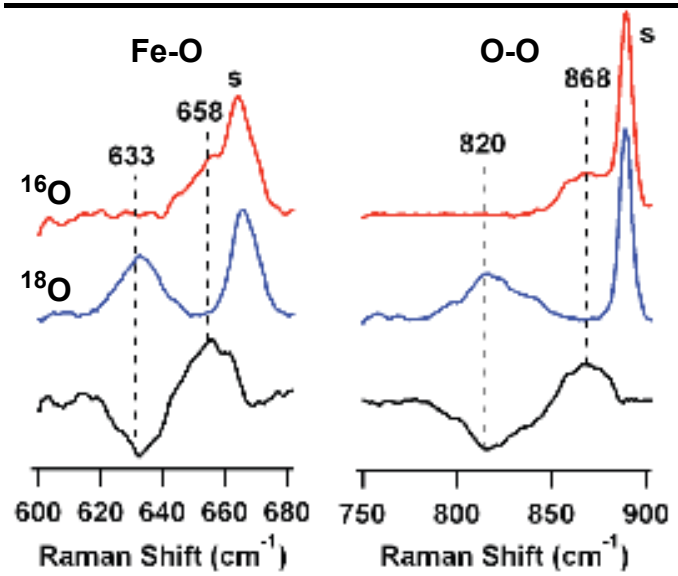

Raman spectrum

O-O stretch (λ_{max}= 868 cm^{-1}) of TMC-Fe-OOH is higher than other high-spin Fe^{III}-OOH(R) complexes and much higher than low-spin Fe^{III}-OOH complexes.

cf) high-spin complex:[Fe(H_2bppa)(OOH)]$^{2+}$ (λ_{max}= 830 cm^{-1})
Inorg. Chem. **2002**, *41*, 616.

low-spin complex: [Fe(N4Py)(OOH)]$^{2+}$ (λ_{max}= 790 cm^{-1})
JACS. **2002**, *124*, 10810.

Fe-O stretch (λ_{max}= 658 cm^{-1}) is higher than six-cordinate high-spin complex (λ_{max}= 621 cm^{-1}), indicating the absence of *trans-axial* ligand.

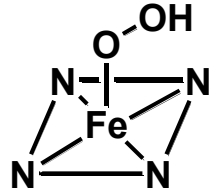

high-spin (S=5/2) Fe^{III} species

Fe=O & Fe-O_2 Complexes formong Fe(IV)=O from Fe-OOH

Which pathway is correct??

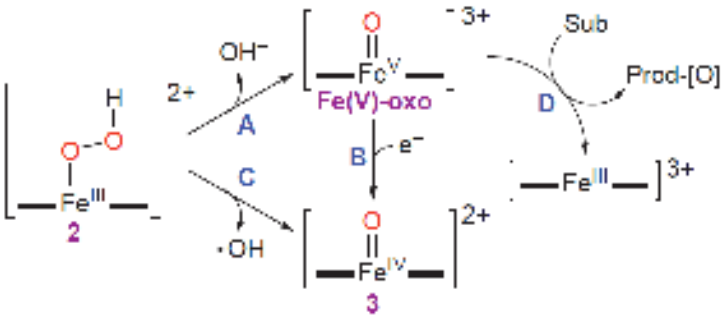

If Fe(IV)=O were in fact product of 1e-reduction of Fe(V)=O, the amount of Fe(IV)=O was decrease due to the fast reaction between the highly reactive Fe(V)=O and the substrates.

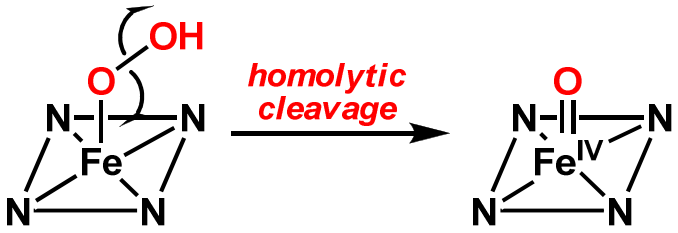

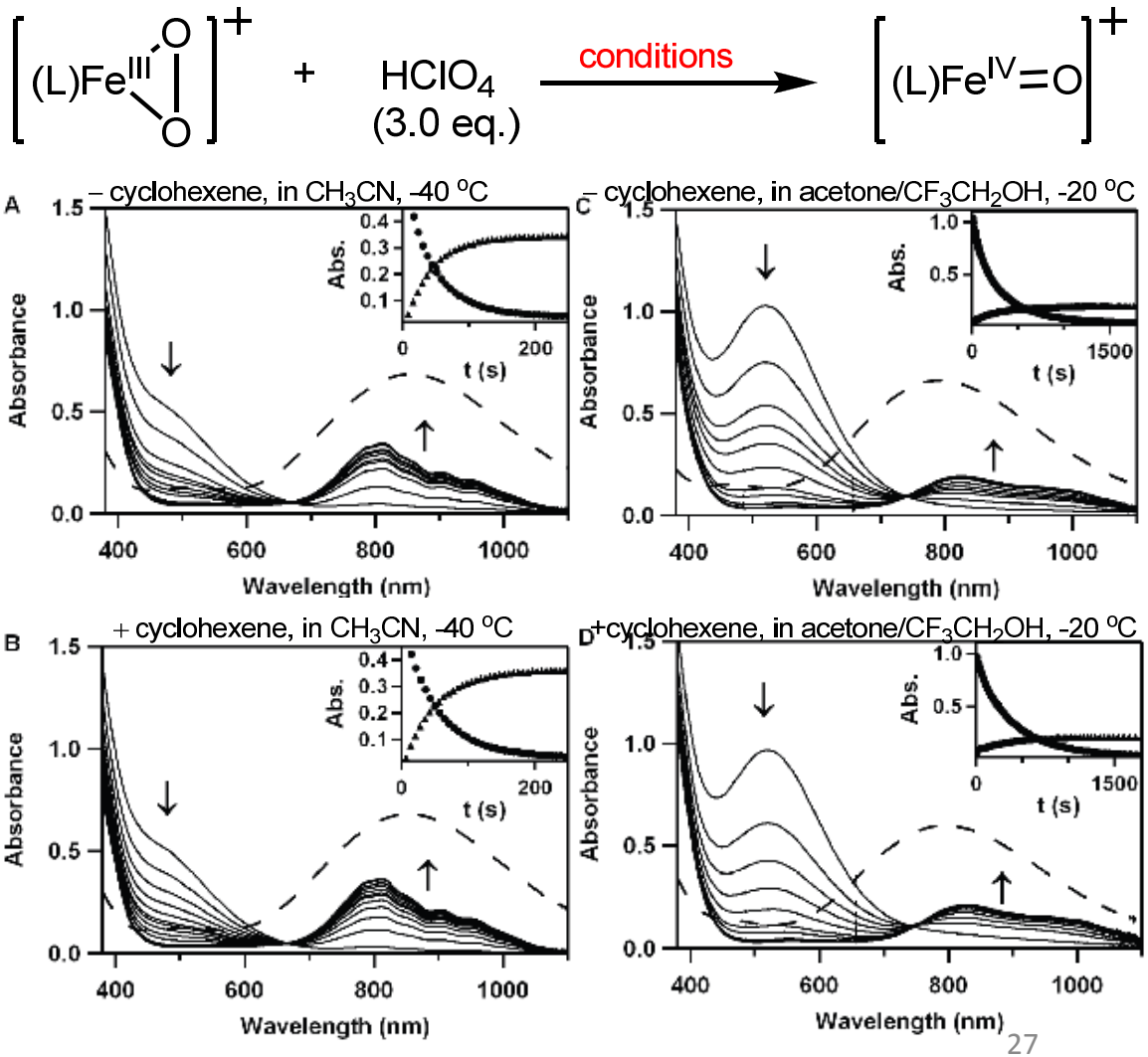

3. Reactivity

A. Electrophilic reaction

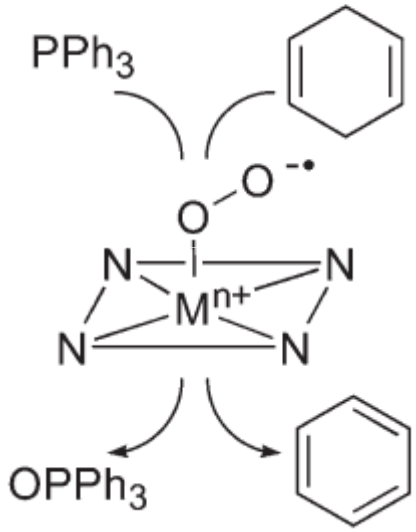

B. Nucleophilic reaction

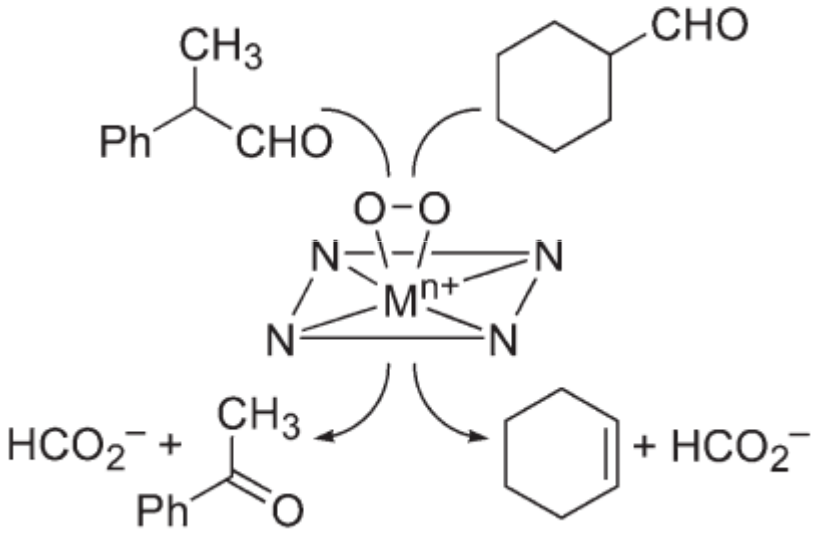

Electrophilic Reaction with Cr-superoxo/C-H activation

JACS, **2010**, *132*, 5958.

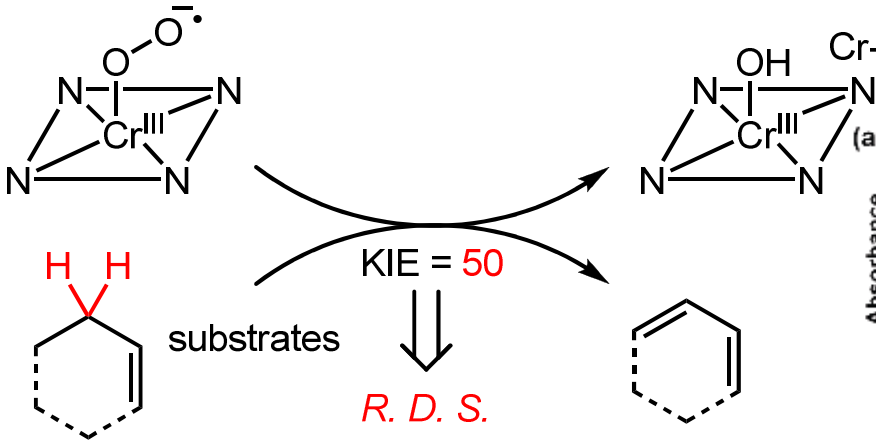

$Cr\text{-}O_2$; pseudo-first order decay & its conctants was dependent on [substrate]. second-order rate constants were determined.

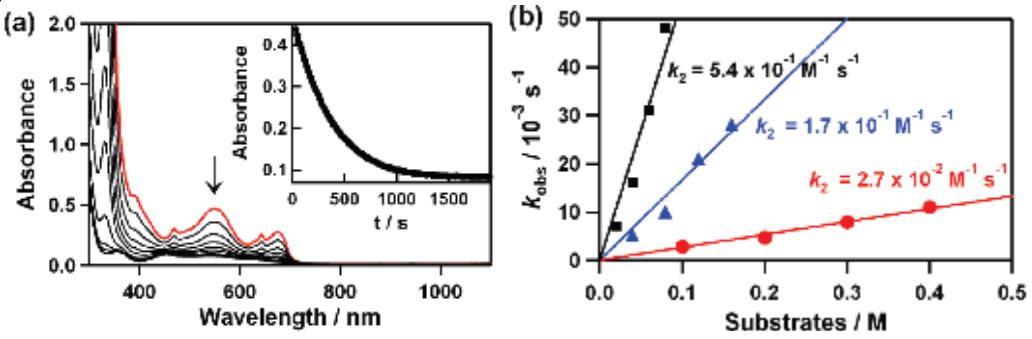

myo-Inositol oxygenase
PNAS. **2004**, *101*, 13105.

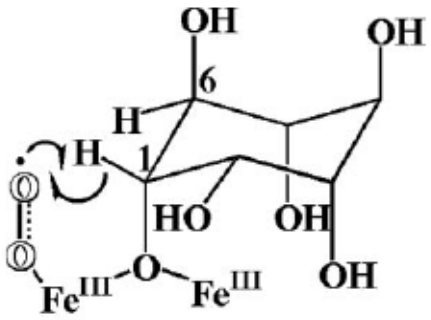

KIE= 8-16

xantane DHA CHD

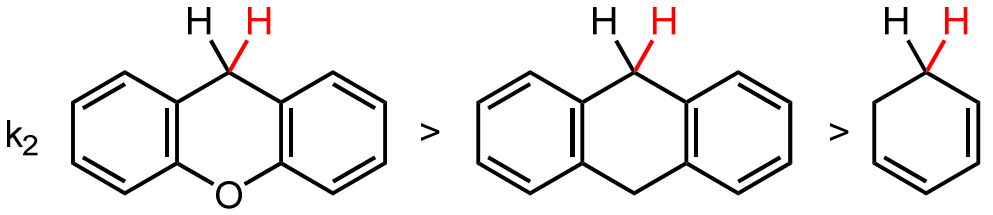

linear corelation !!

BDE 75.5 kcal/mol 77 kcal/mol 78 kcal/mol

Electrophilic Reaction with Cr-superoxo/O-H activation

Chem. Sci. **2011**, 2, 2057.

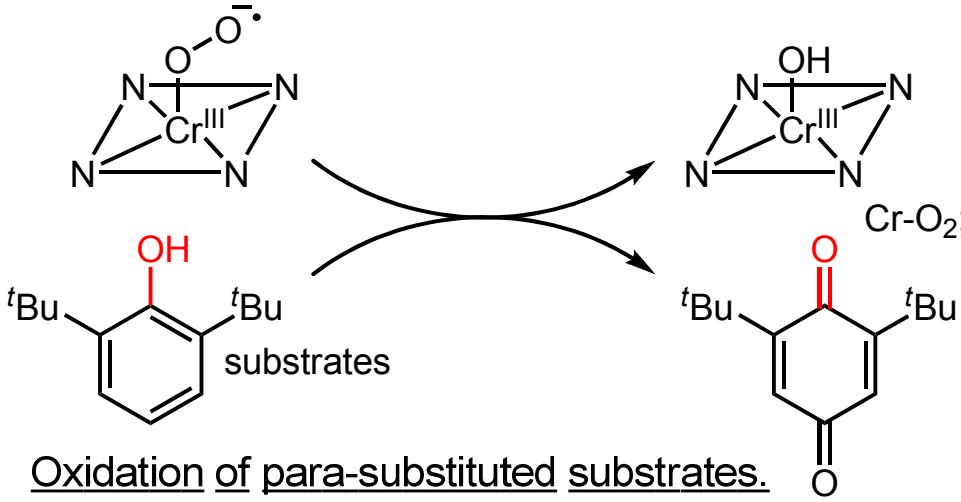

Cr-O_2; pseudo-first order decay & its conctants was dependent on [substrate]. second-order rate constants were determined. (k_2= 4.7 x 10^{-1} ` -40 ^{o}C)

Oxidation of para-substituted substrates.

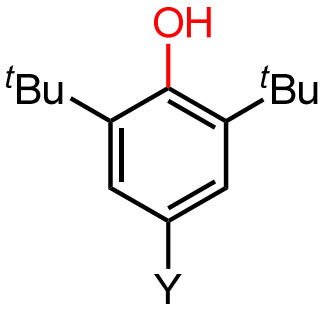

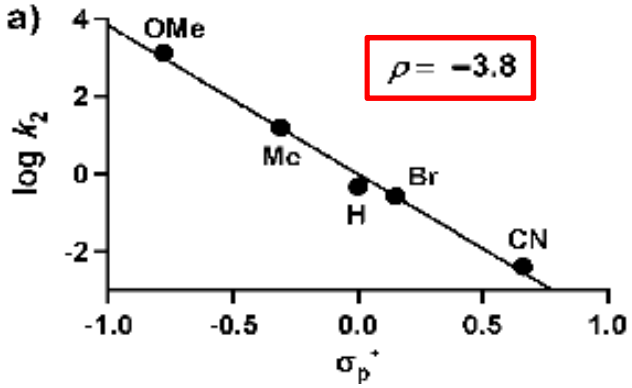

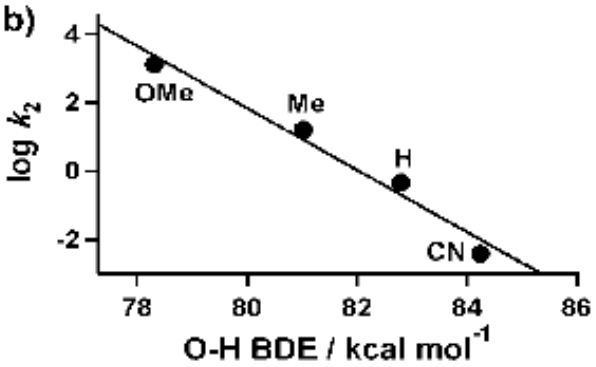

H-atom abstraction is the rate determining step!!

Electrophilic Reaction with Ni(14-TMC)-O2

JACS, **2006**, *128*, 14230.

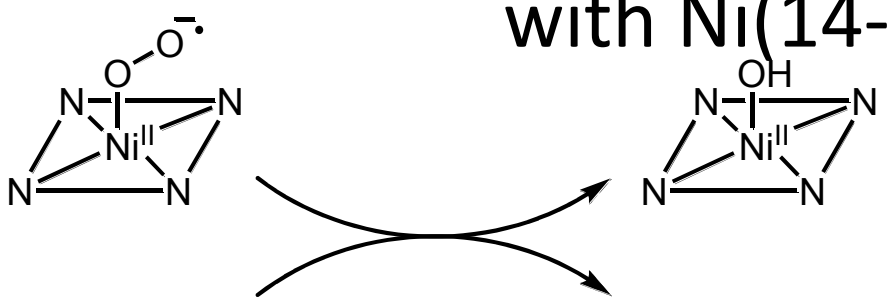

PPh_3 $Ph_3P{=}O$

when Ni-$^{18}O_2$ was used, $^{18}O{=}PPh_3$ was obtained.

⇓

source of O is Ni-O_2

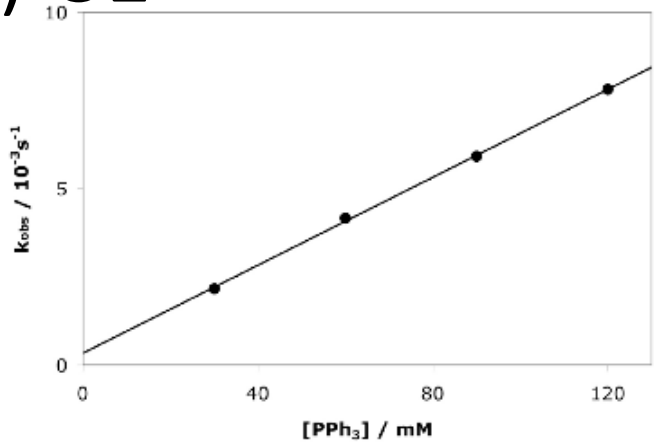

second-order rate constant

k = 6.5 X 10^{-3} $M^{-1}s^{-1}$ at 0 °C

DFT calculation *Chem. Commun*. **2011**, *47*, 10674.

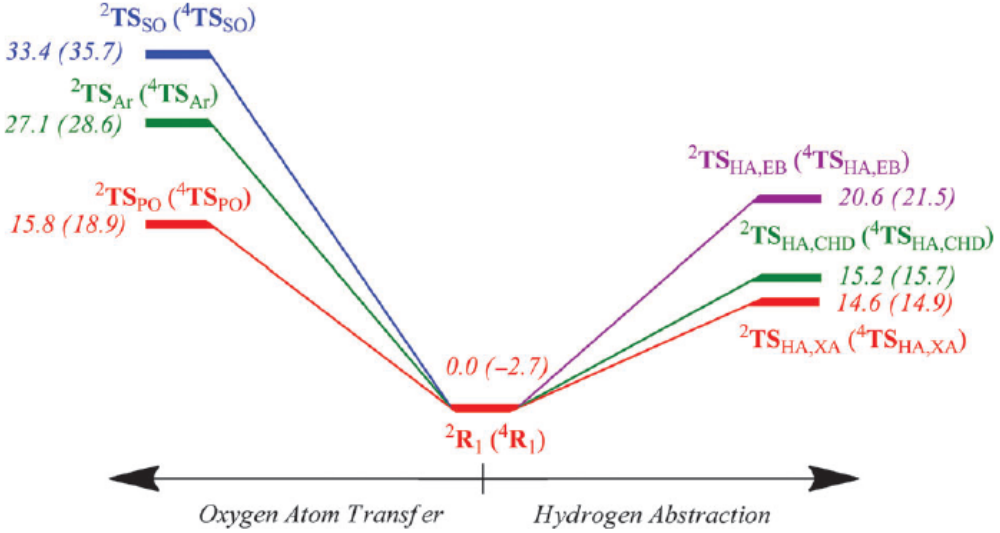

Ni-peroxo complex can oxidaze PPh_3, XA, CHD.

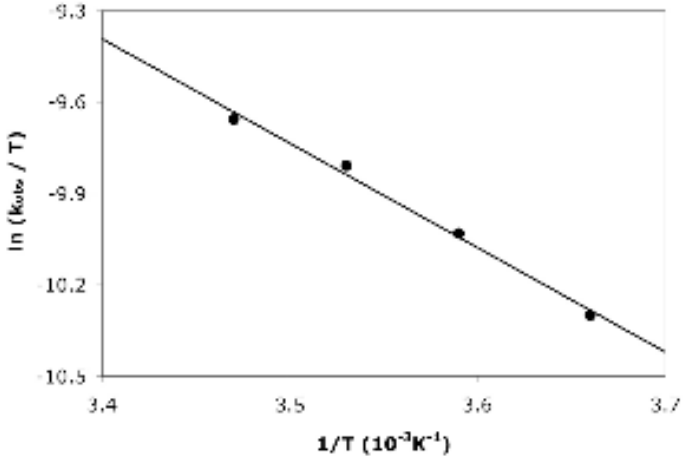

Eyring analysis

$\Delta H^{\ddagger}$ = 6.8 kcal/mol

$\Delta S^{\ddagger}$ = -44 cal $mol^{-1}K^{-1}$

$\Delta G^{\ddagger}$ = 18.8 kcal

O_2 transfer reaction with Ni(12-TMC)-O_2

Nat. Chem. **2009**, *1*, 568.

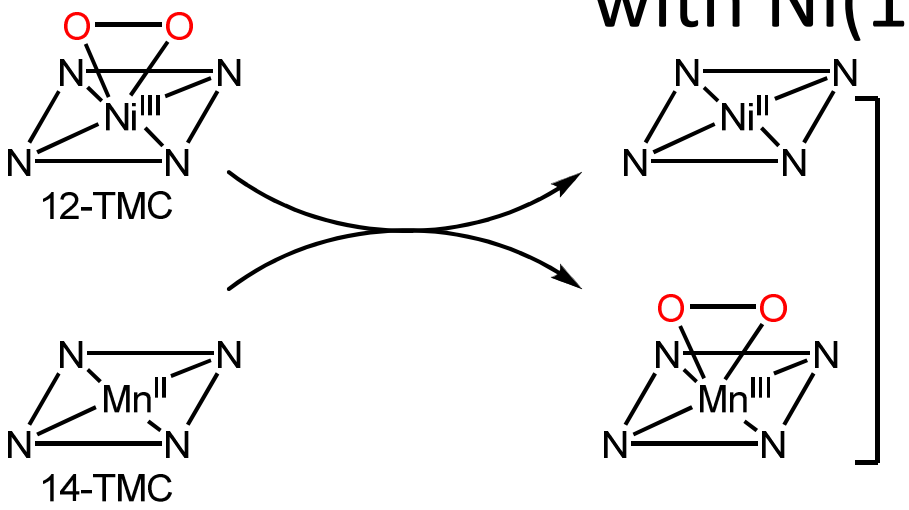

These complexes are confirmed by ESI-MS, UV-vis.

Ni-$^{18}O_2$ gave only Mn-^{18}O complex.

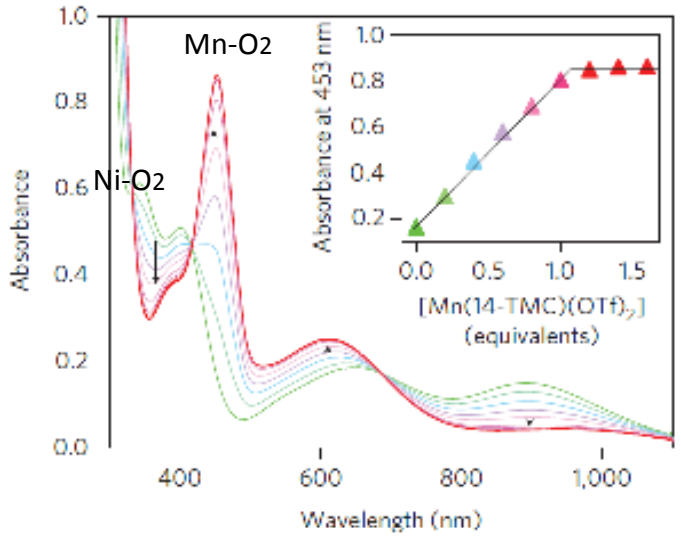

spectral evidence for an intermolecular O_2 transfer from N-O_2 to Mn.

Absorption of reaction

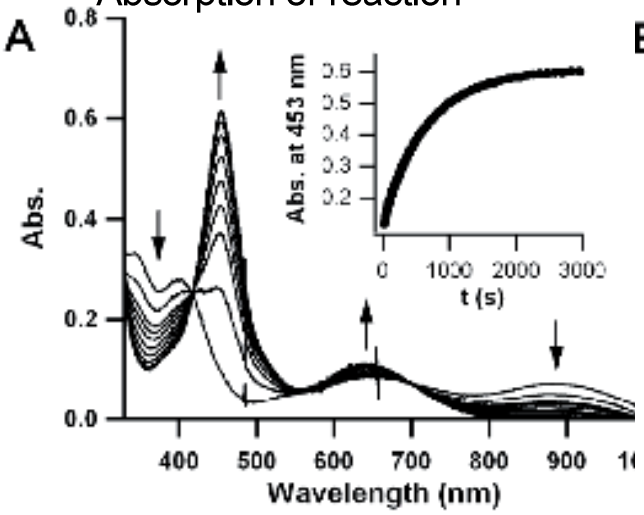

First order decay was observed.

kinetics

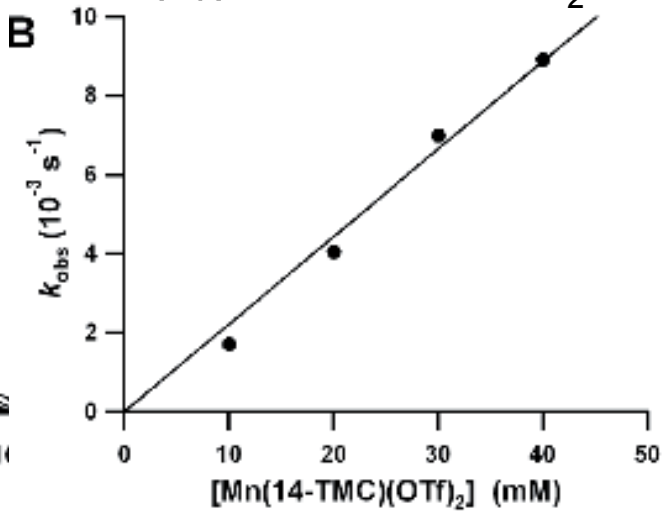

second-order rate constant

k_2= 2.0 X 10-^{1} $M^{-1}s^{-1}$ @ -50 °C

from Eyring plot –60–-30 °C

$\Delta H^{\ddagger}$ = 49 kJ/mol

$\Delta S^{\ddagger}$ = –76 J $mol^{-1}K^{-1}$

$\Delta G^{\ddagger}$ = 22 kJ

⇩

bimolecular mechanism

&

significant -ΔS value means Ni-O-O-Mn formation is R.D.S..

3. Reactivity

A. Electrophilic reaction

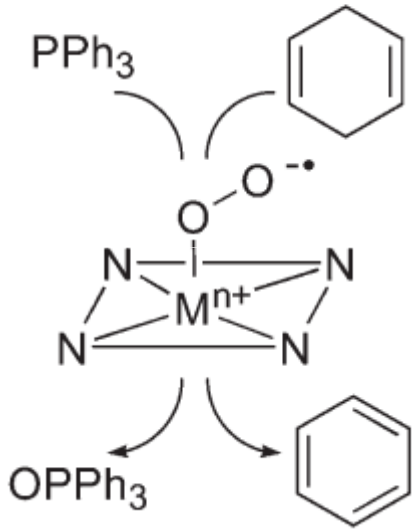

B. Nucleophilic reaction

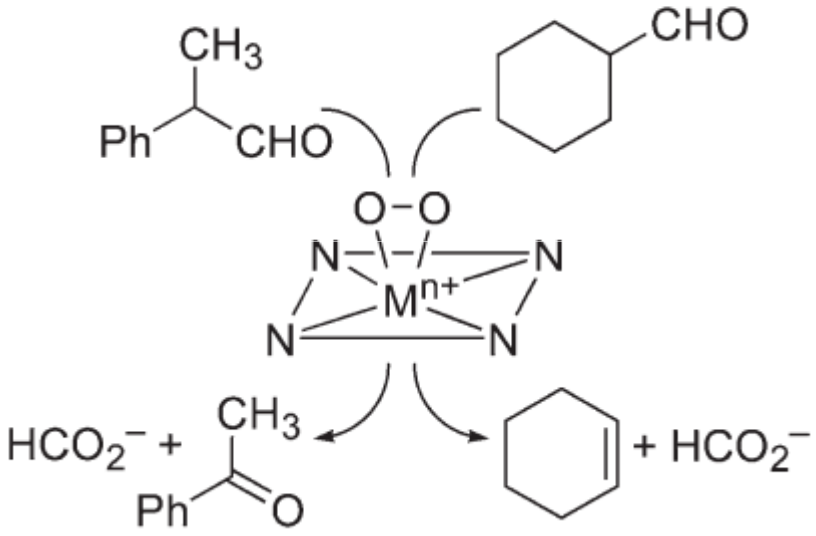

Deformylation
(oxidative nucleophilic addition)

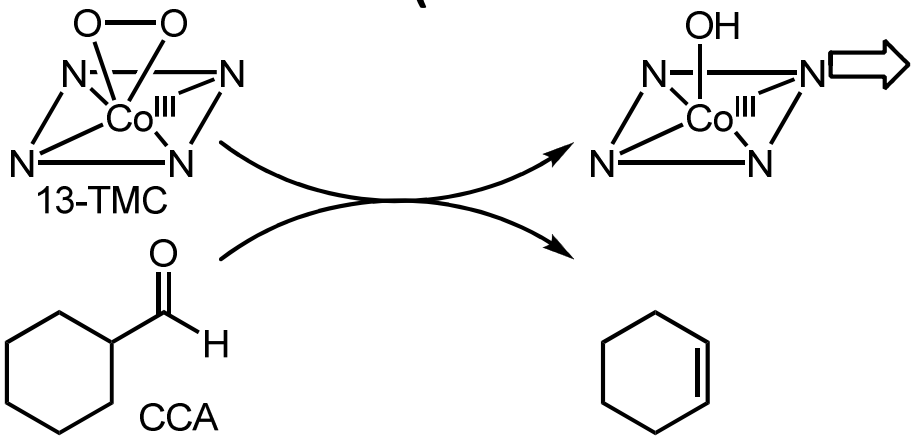

first order generation
k_{obs}= 1.6 X 10^{-2} s^{-1}

second order rate constants
k_2= 1.5 X 10-2 $M^{-1}s^{-1}$ @ 25 °C

Eyring plot; CCA

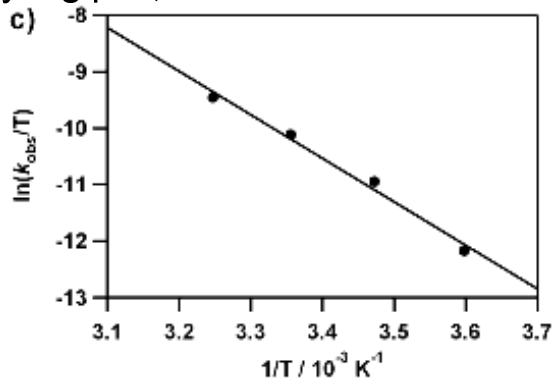

$\Delta H^{\ddagger}$= 64 kJ/mol
$\Delta S^{\ddagger}$= -67 J $mol^{-1}K^{-1}$
$\Delta G^{\ddagger}$= 26 kJ

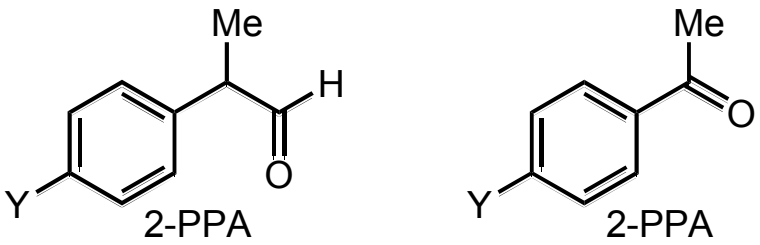

Hammet plot; 2-PPA

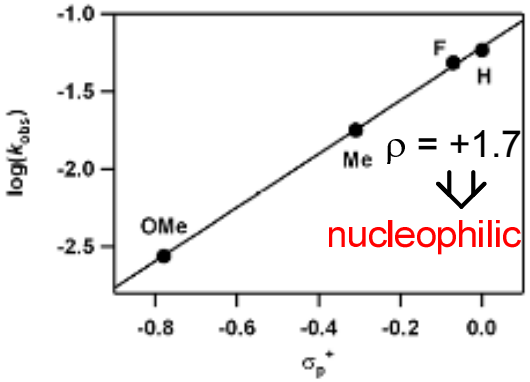

ρ = +1.7

nucleophilic reaction

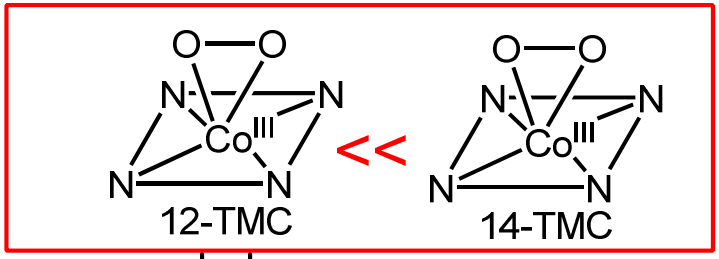

deformylation was observed
but k couldn't be detected.

reactivity

repulsion of O and Me

Deformylation
axial ligand effect

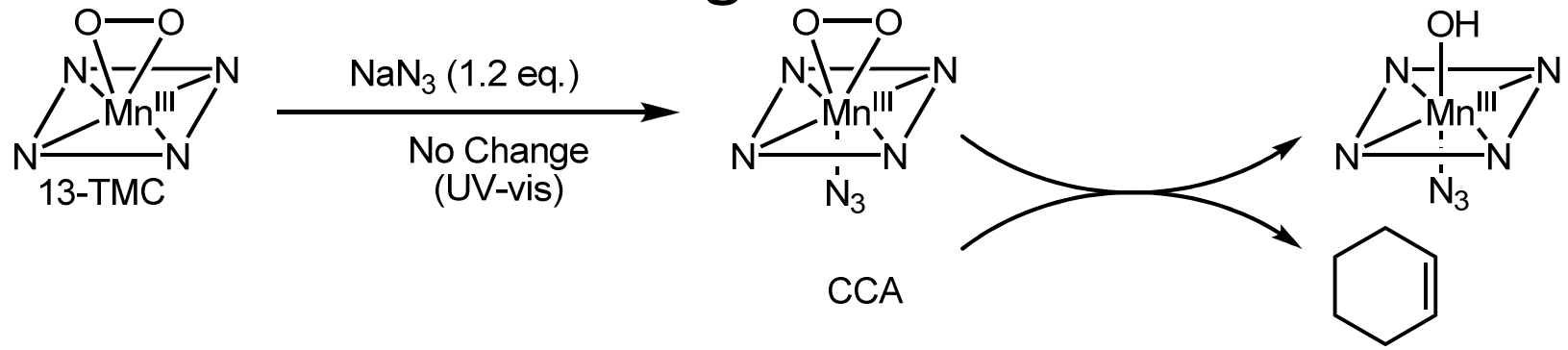

Mn-O_2

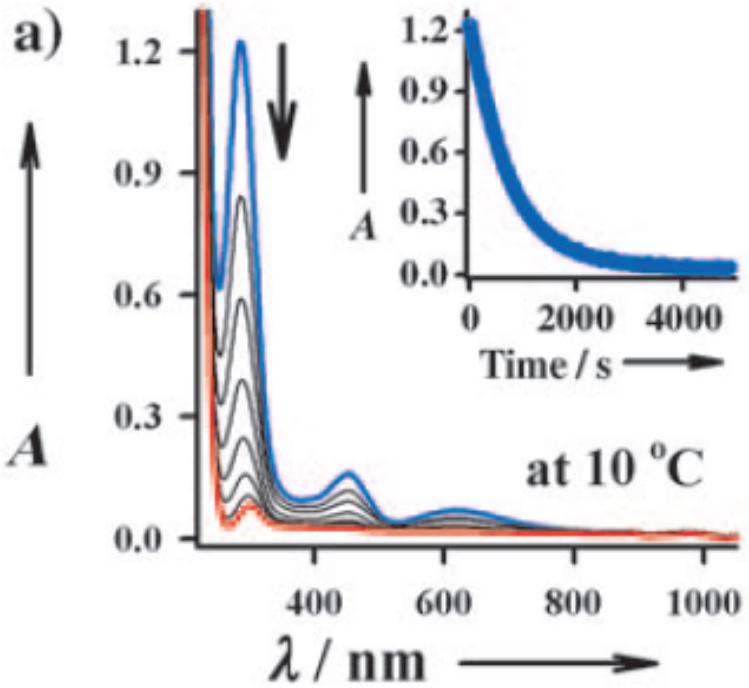

Mn-O_2 + N_3

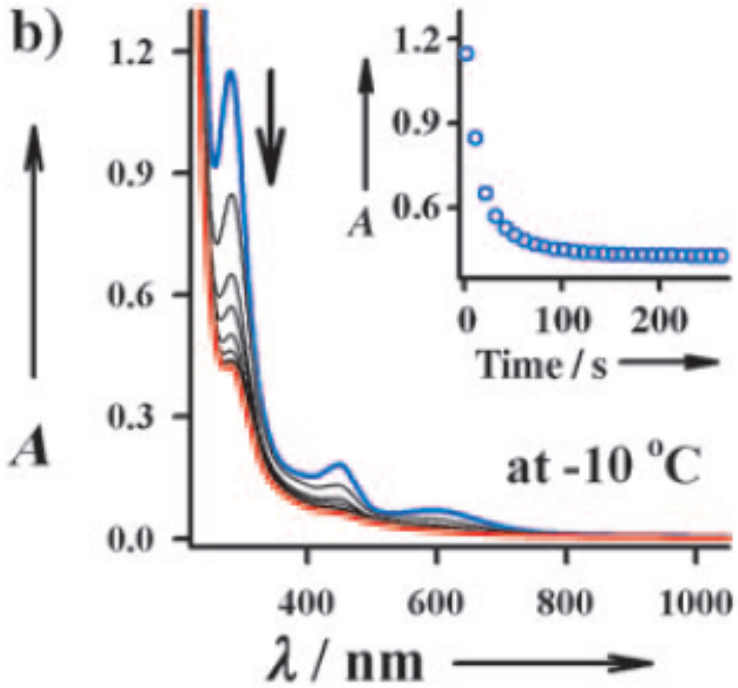

Deformylation
axial ligand effect

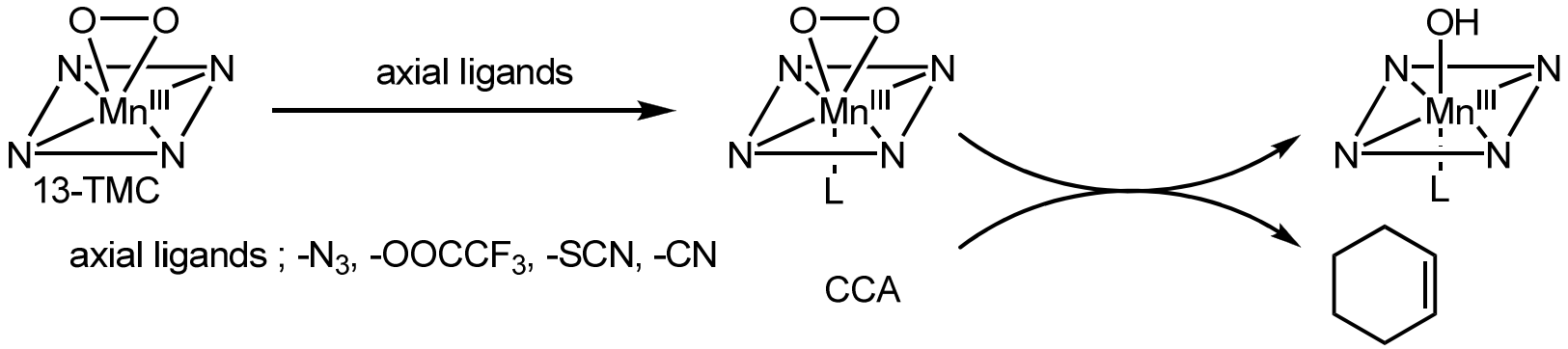

plot of logk_2 against $E_{p,a}$

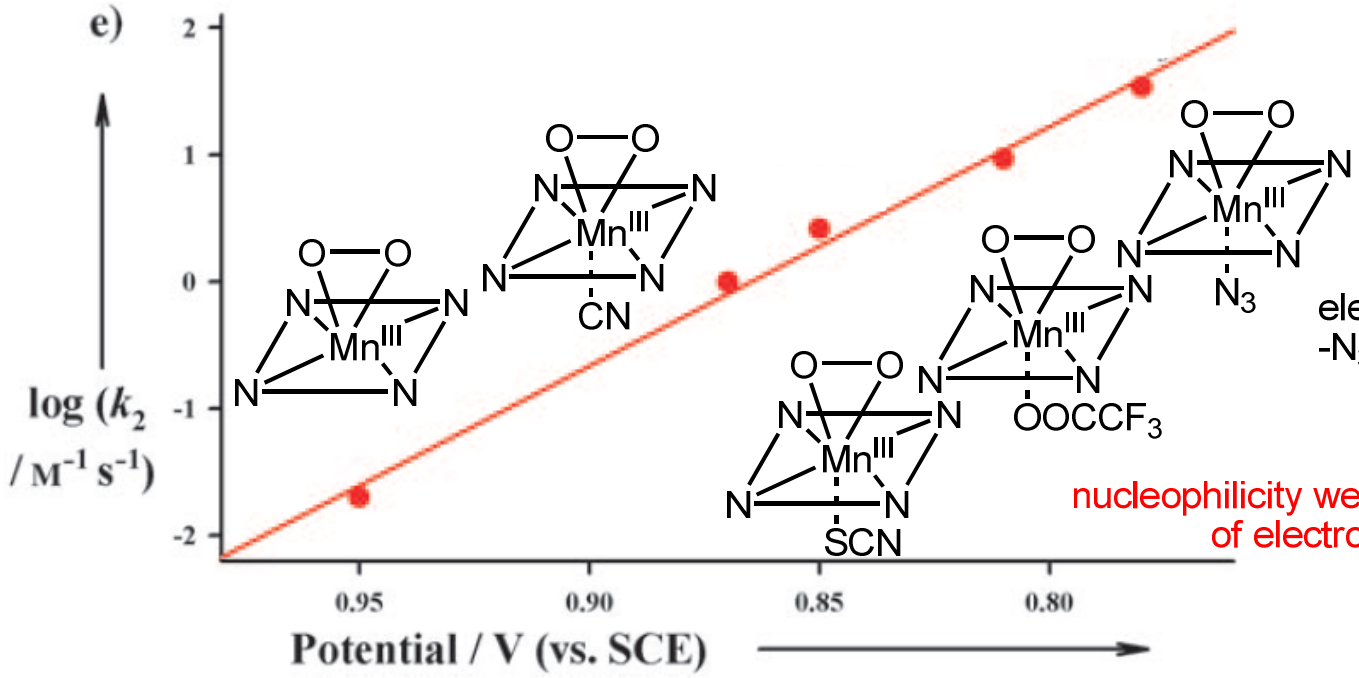

electron richness & reactivity
$-N_3$ > $-OOCCF_3$ > -SCN > -CN > -

nucleophilicity were increased by the coordination of electron-donating axial rigand.

Deformylation
axial ligand effect

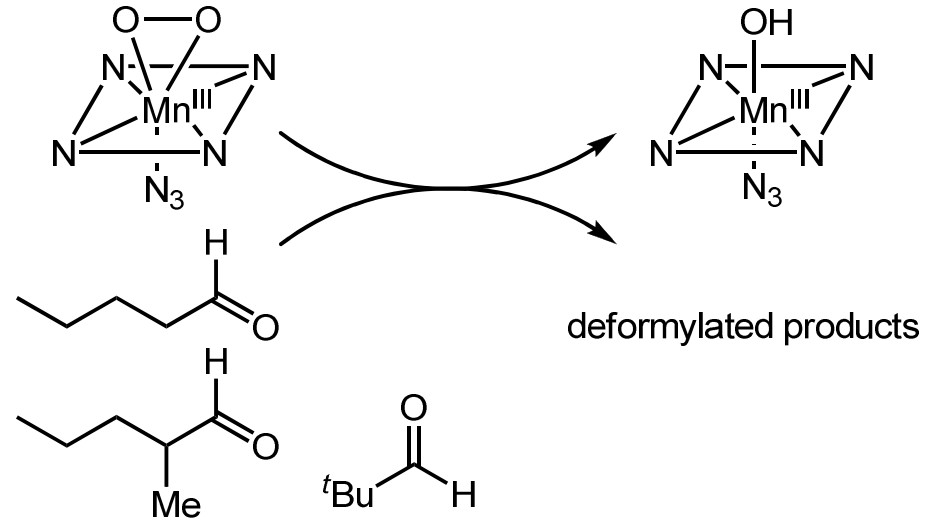

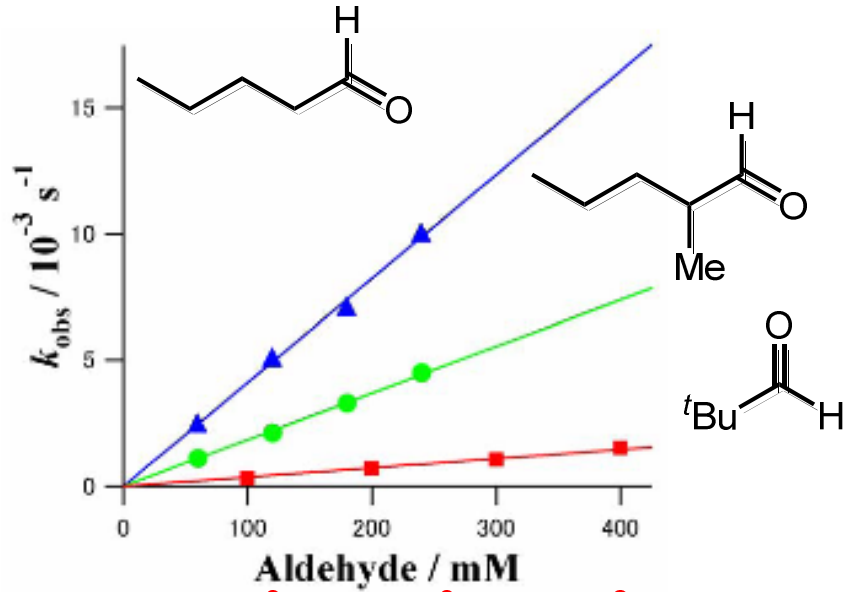

Reactivity; 1^o-CHO > 2^o-CHO > 3^o-CHO

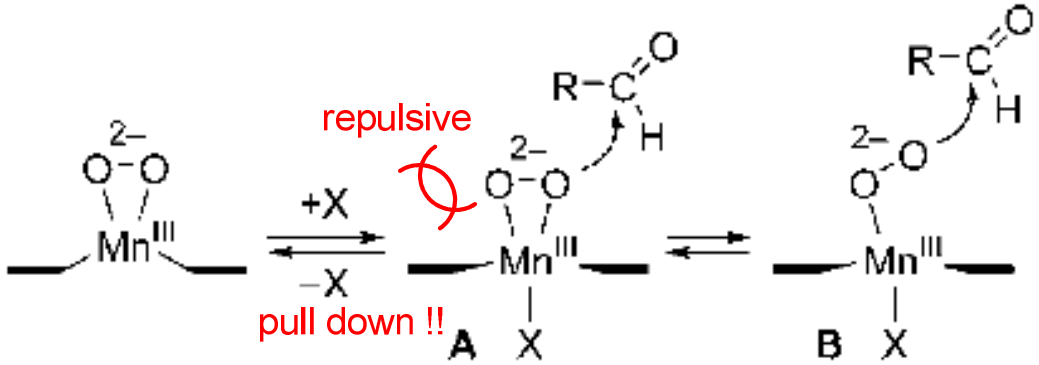

DFT calculation
of anionic character

cf) *Chem. Eur. J.* **2001**, *7*, 4954.
Axial ligand pulls down Mn center.

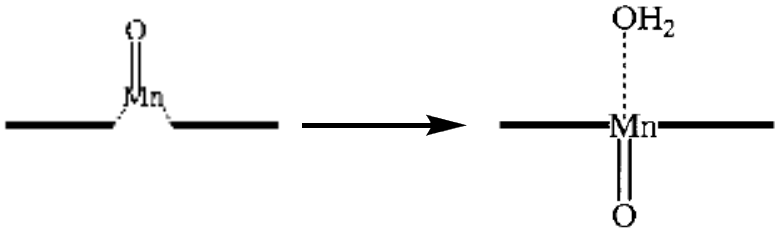

Summary

- M-O_2 complexes have been synthesized & characterized.

- The coordination mode of O_2 are affected by some factors.
  (e.g. ring size of ligand; Ni, pH; Fe-O_2)

- M-O_2 reactivity
  end-on complexes -> electrophilic oxidation
  side-on complexes -> nucleophilic oxidation
  catalytic reaction side-on Fe-O2
  (TON~3)
  nucleophilicity is also affected by ring
  size & axial ligand

Summary of M-O2 & its physical properties

	Chromium	Manganese	Iron	Cobalt	Nickel
14-TMC	1 Cr(III)-superoxo	2  Mn(III)-peroxo	4 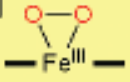 Fe(III)-peroxo	5 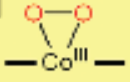 Co(III)-peroxo	8 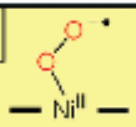 Ni(II)-superoxo
13-TMC		3  Mn(III)-peroxo		6 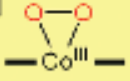 Co(III)-peroxo	
12-TMC		 Mn(III)-peroxo[b]		7 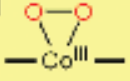 Co(iii)-peroxo	9  Ni(III)-peroxo

entry	$M-O_2$ complex	UV–vis λ [nm] (ε [M^{-1} cm^{-1}])	ESI-MS m/z $^{16}O_2$ (m/z $^{18}O_2$)	rRaman [cm^{-1}] $\nu(^{16}O-^{16}O)$ ($\nu(^{18}O-^{18}O)$)	EPR	spin state	bond lengths M–O/O–O [Å]
1	$[Cr^{III}(14\text{-TMC})(O_2)(Cl)]^+$ (**1**)	331 (3800), 391 (290), 469 (150), 549 (240), 643 (130), 675 (140)	375.0 (379.0)	1170 (1104)	silent	$S = 1$	1.876(4)/1.231(6)
2	$[Mn^{III}(14\text{-TMC})(O_2)]^+$ (**2**)	453 (490), 630 (120)	343.1 (347.1)		silent	$S = 2$	1.884(2)/1.403(4)
3	$[Mn^{III}(13\text{-TMC})(O_2)]^+$ (**3**)	288 (2400), 452 (390), 615 (190)	329.1 (333.1)		silent	$S = 2$	1.859/1.410(4)
4	$[Fe^{III}(14\text{-TMC})(O_2)]^+$ (**4**)	750 (600)	344.1 (348.1)	825 (781)	$g = 8.8$, 5.9, 4.3	$S = 5/2$	1.910/1.463(6)
5	$[Co^{III}(14\text{-TMC})(O_2)]^+$ (**5**)	436 (250), 575 (100), 801 (90)	347.1 (351.1)		silent	$S = 1$	
6	$[Co^{III}(13\text{-TMC})(O_2)]^+$ (**6**)	348 (620), 562 (210), ~500 (170), ~710 (100)	333.1 (337.1)	902 (846)	silent	$S = 0$	1.855/1.438(4)
7	$[Co^{III}(12\text{-TMC})(O_2)]^+$ (**7**)	350 (450), 560 (180), ~500 (150), ~710 (90)	319.1 (323.1)	902 (845)	silent	$S = 0$	1.866/1.4389(17)
8	$[Ni^{II}(14\text{-TMC})(O_2)]^+$ (**8**)	336 (610), 414 (130), 690 (50)	346.1 (350.0)	1131 (1067)	$g = 2.29$, 2.21, 2.09	$S = 1/2$	
9	$[Ni^{III}(12\text{-TMC})(O_2)]^+$ (**9**)	345 (300), 400 (250), 646 (100), 899 (70)	318.0 (322.0)	1002 (945)	$g = 2.22$, 2.17, 2.06	$S = 1/2$	1.889/1.386(4)